Report

Current Biology

A Convergent and Essential Interneuron Pathway for Mauthner-Cell-Mediated Escapes

Graphical Abstract

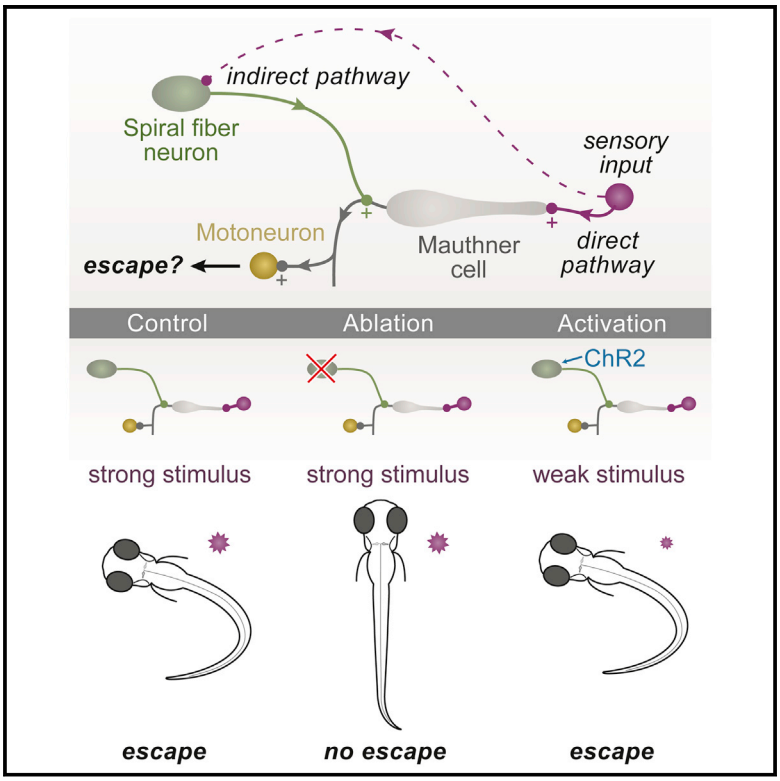

Authors

Alix M.B. Lacoste, David Schoppik, ..., Florian Engert, Alexander F. Schier

Correspondence

schier@fas.harvard.edu

In Brief

Lacoste et al. find that excitatory interneurons form an essential feedforward pathway for the Mauthner-cell-mediated startle behavior of larval zebrafish. Together with direct sensory afferents on the lateral dendrites, the input of spiral fiber neurons at the axon hillock of the Mauthner cell enables fast escapes in response to noxious stimuli.

Highlights

- Spiral fiber neurons excite Mauthner cells, which mediate fast escape behavior
- Calcium imaging reveals that spiral fiber neurons encode aversive sensory cues
- Ablation and optogenetic experiments indicate that they are essential for escapes
- This study uncovers the crucial role of a feedforward excitatory motif for behavior

Lacoste et al., 2015, Current Biology *25*, 1526–1534
June 1, 2015 ©2015 Elsevier Ltd All rights reserved
http://dx.doi.org/10.1016/j.cub.2015.04.025

CellPress

Current Biology
Report

A Convergent and Essential Interneuron Pathway for Mauthner-Cell-Mediated Escapes

Alix M.B. Lacoste,[1] David Schoppik,[1,7] Drew N. Robson,[1,8] Martin Haesemeyer,[1] Ruben Portugues,[1,9] Jennifer M. Li,[1,8] Owen Randlett,[1] Caroline L. Wee,[2] Florian Engert,[1] and Alexander F. Schier[1,3,4,5,6,*]
[1]Department of Molecular and Cellular Biology, Harvard University, Cambridge, MA 02138, USA
[2]Program in Neuroscience, Harvard Medical School, Boston, MA 02115, USA
[3]Center for Brain Science, Harvard University, Cambridge, MA 02138, USA
[4]Broad Institute of MIT and Harvard, Cambridge, MA 02142, USA
[5]Harvard Stem Cell Institute, Cambridge, MA 02138, USA
[6]FAS Center for Systems Biology, Harvard University, MA 02138, USA
[7]Present address: Neuroscience Institute, New York University Langone School of Medicine, New York, NY 10016, USA
[8]Present address: Rowland Institute at Harvard, Cambridge, MA 02142, USA
[9]Present address: Max Planck Institute of Neurobiology, 82152 Martinsried, Germany
*Correspondence: schier@fas.harvard.edu
http://dx.doi.org/10.1016/j.cub.2015.04.025

SUMMARY

The Mauthner cell (M-cell) is a command-like neuron in teleost fish whose firing in response to aversive stimuli is correlated with short-latency escapes [1–3]. M-cells have been proposed as evolutionary ancestors of startle response neurons of the mammalian reticular formation [4], and studies of this circuit have uncovered important principles in neurobiology that generalize to more complex vertebrate models [3]. The main excitatory input was thought to originate from multisensory afferents synapsing directly onto the M-cell dendrites [3]. Here, we describe an additional, convergent pathway that is essential for the M-cell-mediated startle behavior in larval zebrafish. It is composed of excitatory interneurons called spiral fiber neurons, which project to the M-cell axon hillock. By in vivo calcium imaging, we found that spiral fiber neurons are active in response to aversive stimuli capable of eliciting escapes. Like M-cell ablations, bilateral ablations of spiral fiber neurons largely eliminate short-latency escapes. Unilateral spiral fiber neuron ablations shift the directionality of escapes and indicate that spiral fiber neurons excite the M-cell in a lateralized manner. Their optogenetic activation increases the probability of short-latency escapes, supporting the notion that spiral fiber neurons help activate M-cell-mediated startle behavior. These results reveal that spiral fiber neurons are essential for the function of the M-cell in response to sensory cues and suggest that convergent excitatory inputs that differ in their input location and timing ensure reliable activation of the M-cell, a feedforward excitatory motif that may extend to other neural circuits.

RESULTS

Activity in Mauthner cells (M-cells), a pair of large neurons located bilaterally in the hindbrain and projecting directly to motoneurons, is associated with escapes of short latencies [5–8]. Spiral fiber neurons are a group of neurons that project to the contralateral M-cell [9], where they wrap around the axon hillock at a structure called the axon cap [10]. Previous studies suggest that spiral fiber neurons excite the M-cell in adult goldfish [11], and stimulation of a single spiral fiber neuron in larval zebrafish is capable of eliciting an excitatory post-synaptic potential (EPSP) in the contralateral M-cell [9]. Anatomical [10], as well as electrophysiological and pharmacological [9], evidence points to the presence of both glutamatergic and electrical synapses between spiral fiber neurons and the M-cell. Based on these studies, spiral fiber neurons are well positioned to influence the M-cell-mediated escape behavior. In fact, mutants for the *retinoblastoma-1* gene that have defects in axon targeting, including in the spiral fiber neurons, display abnormal turning movements in response to touch [12, 13]. However, the stimuli that drive the spiral fiber neurons have yet to be identified and their role in the M-cell escape network remain unclear. Here, we address these questions using functional calcium imaging, ablations, optogenetics, and behavior analysis.

Spiral Fiber Neurons Respond to Aversive Stimuli

We used a transgenic line, *Tg(–6.7FRhcrtR:gal4VP16)*, that labels spiral fiber neurons and other neurons in the larval zebrafish brain (Figure 1A, Movie S1, and the Supplemental Experimental Procedures). In 5-day-old larval zebrafish, spiral fiber neurons are a group of approximately ten neurons located bilaterally in rhombomere 3, rostro-ventral of the M-cells. These neurons all have descending projections to the contralateral M-cell axon cap and do not appear to contact other targets [9]. We first asked whether spiral fiber neurons are capable of sensing stimuli that are classically used to elicit M-cell-dependent escapes (Figure 1B). In paralyzed animals embedded in agarose, we monitored calcium dynamics in spiral fiber neurons

 ©2015 Elsevier Ltd All rights reserved

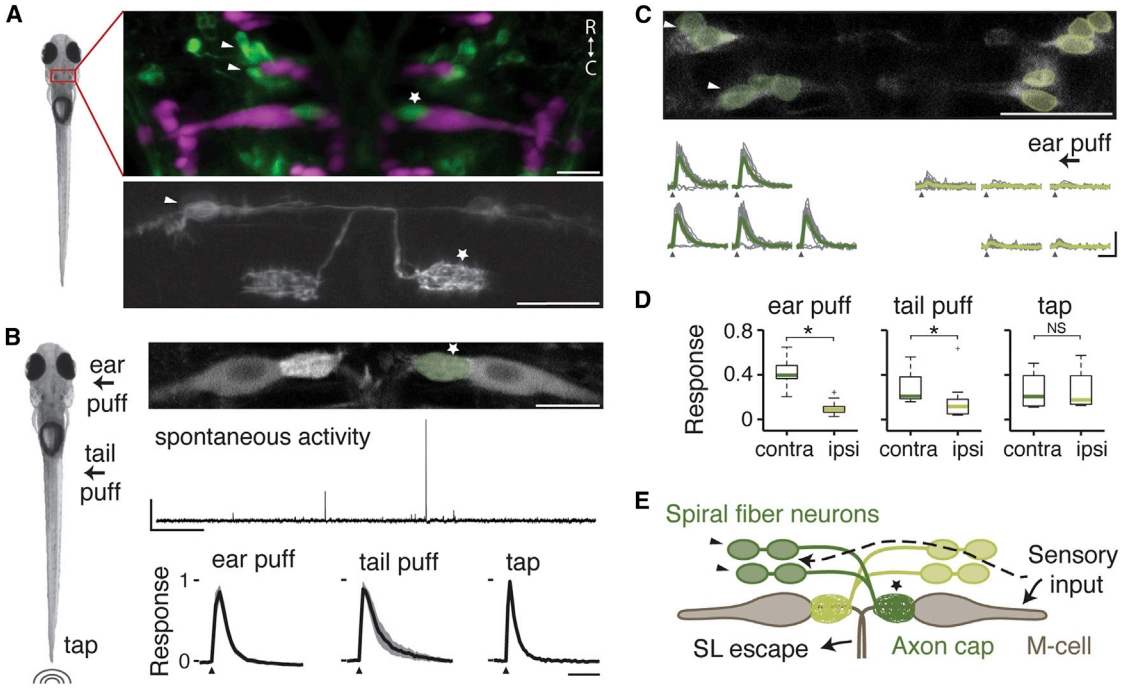

Figure 1. Spiral Fiber Neurons Respond to Aversive Stimuli

(A) Left: 5-day-old zebrafish larvae. Top: *Tg(–6.7FRhcrtR:gal4VP16)*; *Tg(UAS:GCaMP5)* labels spiral fiber neurons (arrowhead) among other neurons. The M-cell and other reticulospinal neurons are labeled with tetramethylrhodamine dextran by reticulospinal backfill. Spiral fiber neuron cell bodies are located in rhombomere 3 in two rostro-caudal (R↔C) clusters, approximately 25–40 μm rostral, 5–15 μm lateral, and 0–20 μm ventral of the axon cap (star). They all have axons descending contralaterally into the axon cap of the M-cell. Bottom: transient expression of membrane-targeted GFP (*UAS:GAP43-GFP*) in *Tg(–6.7FRhcrtR:gal4VP16)* labels two spiral fiber neurons on the left and one spiral fiber neuron on the right that project to the contralateral M-cell axon cap.

(B) Left: three different stimuli were delivered to paralyzed zebrafish larvae—water puffs directed at the right ear, water puffs directed at the right side of the tail, and non-directional taps delivered onto the dish holding the fish. Top: projection of two-photon image stack showing M-cells and spiral fiber neuron axon terminals labeled with the calcium indicator *Tg(UAS:GCaMP-HS)* driven by *Et(fos:Gal4-VP16)s1181t* and *Tg(–6.7FRhcrtR:gal4VP16)*, respectively. middle: Typical spontaneous activity in the spiral fiber neuron axon terminals. Scale bars represent 5 min horizontally and1 Δf/f vertically. Bottom: mean response amplitude in the right spiral fiber neuron axon terminals for different stimuli: ear puffs (n = 7, left), tail puffs (n = 5, center), and taps (n = 6, right). For each fish, the change in fluorescence (Δf/f) from trials in which the axon cap was active was normalized to the maximum Δf/f across trials and then averaged. The black line is the mean across fish with the SEM shaded. Stimulus delivery is indicated by an arrowhead. The horizontal scale bar represents 2 s.

(C) Top: single recording plane showing spiral fiber neuron somata in *Tg(–6.7FRhcrtR:gal4VP16)*; *Tg(UAS:GCaMP-HS)*. Bottom: mean Δf/f across trials in green and individual trials in gray for spiral fiber neuron somata from the top panel located on the left (dark green) and on the right (light green) responding to a water puff delivered to the right ear (arrow). Contralateral spiral fiber neurons respond to the stimulus, but ipsilateral spiral fiber neurons do not. Traces in which spiral fiber neurons on the left do not respond correspond to the same trials. Note that while caudal neurons seem to respond before rostral neurons, this is an artifact of the delay introduced by two-photon line scanning. Scale bars represent 2 s horizontally and 2 Δf/f vertically.

(D) Boxplot showing the normalized response of spiral fiber neurons across fish. Response was defined as the area under the Δf/f curve over a 1.5 s response window. This was normalized for each cell to the maximum response observed in a given experiment, and then cells located on the contralateral and ipsilateral side with respect to the stimulus were averaged. Green lines are the medians across fish, box edges are the 25th and 75th percentiles, the whiskers extend to the most extreme data points not considered outliers, and crosses are outliers. The following stimuli were delivered: ear puffs (left; n = 10 fish, $p = 2.5 \times 10^{-4}$), tail puffs (center; n = 10, p = 0.02), and taps (right; n = 4, p = 0.89). *$p < 0.05$; NS, not significant by Wilcoxon rank-sum test.

(E) Model showing the M-cells receiving ipsilateral sensory input, which includes auditory/vestibular afferents onto the lateral dendrite. Our results suggest that spiral fiber neuron somata receive similar sensory information from the contralateral side.

Pictures are oriented rostral up. Scale bars represent 20 μm. Arrows point to spiral fiber neuron somata, and a star indicates spiral fiber neuron terminals at the M-cell axon cap. Contra, contralateral; ipsi, ipsilateral; SL, short latency. See also Figure S1 and Movie S1.

labeled with the genetically encoded calcium indicator GCaMP-HS [14] by two-photon microscopy. We first assessed activity in the spiral fiber neuron axon terminals that wrap around the M-cell axon hillock. We observed irregular and infrequent spontaneous activity in spiral fiber neurons, at a rate of about one calcium event per minute (Figure 1B). We then stimulated the animals with three different stimuli: two tactile stimuli consisting of short water pulses delivered either to the otic vesicle (which develops into the ear) [7] or to the tail [6, 15], and a third stimulus that was a primarily auditory/vibrational stimulus consisting of an abrupt tap on the dish holding the animal (similar to [8]). We observed that all three types of stimuli elicited robust responses in the spiral fiber neuron axon terminals (Figure 1B). These responses were independent of M-cell activity: after bilateral M-cell ablations, spiral fiber neurons continued to respond to the tap stimulus with comparable amplitude (Figure S1). Thus, spiral fiber neurons encode a range of sensory information.

M-cells respond to stimuli arriving ipsilaterally on their dendrites, but individual spiral fiber neurons cross the midline and

project to the contralateral M-cell. We thus asked whether the responses of spiral fiber neurons were lateralized accordingly. Consistent with their contralateral projections, we observed that spiral fiber neuron somata were strongly activated by ear and tail stimuli delivered on the contralateral side (Figures 1C and 1D). Ipsilateral spiral fiber neurons also responded but more weakly (ear stimuli: $n = 10$ fish, $p < 0.05$, contralateral versus ipsilateral; tail stimuli: $n = 10$, $p < 0.05$; Wilcoxon rank-sum test), an effect most likely due to directional stimuli also being capable of stimulating the opposite side of the skin to a lesser extent. Responses to the non-directional tap stimulus, on the other hand, were not lateralized (Figure 1D, $n = 4$, $p > 0.05$). These results indicate that spiral fiber neurons receive contralateral sensory input and that as they cross the midline, the laterality of sensory information is preserved across M-cell inputs (Figure 1E).

Spiral Fiber Neuron Ablations Largely Abolish M-Cell-Dependent Short-Latency Escapes

To investigate whether spiral fiber neurons affect the escape behavior, we built an apparatus designed to elicit and quantify escapes in response to an aversive stimulus. 5- to 7-day old fish were embedded in agarose, and their tails were freed. A mechanical tapper hit the plate onto which the fish was placed, in a similar manner to the tap stimulus used for calcium imaging experiments. By imaging at 1,000 Hz, we were able to reconstruct the curvature of the tail as a function of time and to measure the direction, angle, and latency of the response (Figure 2A). The tap stimulus elicited responses with 100% probability ($n = 50$ larvae). The vast majority (99.7%) of these responses were escapes, with latencies ranging from 5–25 ms (9.9 ± 0.19 ms, mean ± SEM). Characteristic escapes consisted of a sharp-angle C-bend of the tail (>60°), followed by a counter turn in the opposite direction and subsequent swimming lasting hundreds of milliseconds (Figure 2A). In accordance with previous findings [8, 16], we classified escapes as either short latency (≦12 ms) or long latency (13–25 ms). Larvae produced short-latency escapes with a high probability (92% ± 1.4%), whereas long-latency escapes were observed infrequently (8.2% ± 1.4%). Responses with latencies above 25 ms (0.26% ± 0.19%) corresponded to other types of movements, such as swims and turns. To uncover the types of sensory systems activated by the tap stimulus, we measured tap responses in fish with non-functional hair cells (*mariner* mutants [17]) and in fish in which the lateral line was ablated by neomycin treatment [18]. Our results indicate that short-latency escapes, but not long-latency escapes, are primarily mediated by the ear, whereas the lateral line does not play a role (Figure S2). Thus, tap stimuli engage several sensory systems, including the ear.

To analyze the respective contributions of the M-cell and spiral fiber neurons to the escape behavior, we compared the response to taps of larvae before and after three ablation conditions: M-cells (Figure 2B), spiral fiber neurons (Figure 2E), or ablation of other neurons in the area as a control (Figure 2H). Targeted ablations were carried out using a pulsed infrared laser as described previously [19]. Previous studies have shown that short-latency escapes in response to auditory stimuli require the M-cells, but tactile stimuli only partially depend on the M-cells [6, 7, 15, 20]. Two sets of segmental homologs are thought to elicit escapes of longer latency when the M-cell does not fire [6, 7, 21]. Thus, due to the multisensory nature of our stimulus, we expected the M-cells to be partially required for short-latency escapes. Indeed, we found that after M-cell ablations, the number of short-latency escapes performed decreased in favor of long-latency escapes ($n = 14$ fish; Figure 2C). The mean probability of short-latency escapes decreased on average 1.8-fold, and long-latency escapes increased 3-fold ($p < 0.05$, Wilcoxon signed-rank test; Figure 2D). Spiral fiber neuron ablations had a similar effect: after ablations, the majority of escapes observed were long latency (Figure 2F). Short-latency escapes were reduced by 6-fold, and long-latency escapes increased 8.1-fold ($n = 13$, $p < 0.05$; Figure 2G). Control ablations did not induce a change in the escape latency profile (Figure 2I) or probability of escapes ($n = 23$, $p > 0.05$; Figure 2J). The overall probability of response was not affected by any of the ablation procedures (Figures 2D, 2G, and 2J).

To compare the effect of ablation across groups, we evaluated the change in short-latency escape probability after ablations. The effects of M-cell and spiral fiber neuron ablations were significantly different from controls ($p < 0.05$, Wilcoxon rank-sum test; Figure 2K). A fraction of M-cell ablations did not produce a strong effect, most likely due to compensatory escape pathways. Nevertheless, the effects of M-cell and spiral fiber neuron ablations were not statistically distinguishable from each other ($p > 0.05$). Taken together, these experiments show that the phenotype after ablation of spiral fiber neurons is similar to that of ablation of M-cells, indicating that spiral fiber neurons play an essential role in M-cell-mediated escapes.

Spiral Fiber Neurons Are Involved in the Laterality of M-Cell-Mediated Escapes

M-cells provide excitation to the contralateral side of the spinal network, resulting in contralateral tail bends. Due to inhibition [22, 23], only one of the two M-cells elicits an escape response at any one time. In accordance with this circuit design, previous studies have shown that after unilateral M-cell ablation, the probability of contralateral short-latency escape is decreased, with a concomitant increase in ipsilateral short-latency escapes [8]. Since spiral fiber neurons project to one M-cell only, we asked whether they also affect the escape behavior in a lateralized manner. To test this, we compared the effect of unilateral M-cell (Figure 3B) and spiral fiber neuron (Figure 3C) ablations on the directionality of the escape behavior in response to non-directional tap stimuli (Figure 3A). We expected that following the anatomy of the circuit, ablation of one M-cell or its contralateral spiral fiber neurons would bias escapes toward the ipsilateral and contralateral side with respect to the ablated somata, respectively (Figure 3E). We found that the overall frequency of short-latency escapes did not change after M-cell ablations (Figure 3D). However, as expected, unilateral M-cell ablations biased escapes toward one side (Figure 3F). Regardless of the original directional preference of individual fish before ablations, in all cases short-latency escapes contralateral to the ablated M-cell were virtually eliminated ($n = 11$, 35% ± 9.0% pre to 7.0% ± 3.6% post; Figure 3G). The directionality of the other, infrequent types of responses, such as long-latency escapes and swims, was not affected by the ablations (data not shown). Unilateral ablation of spiral fiber neurons had a similar effect as ablation of the

 ©2015 Elsevier Ltd All rights reserved

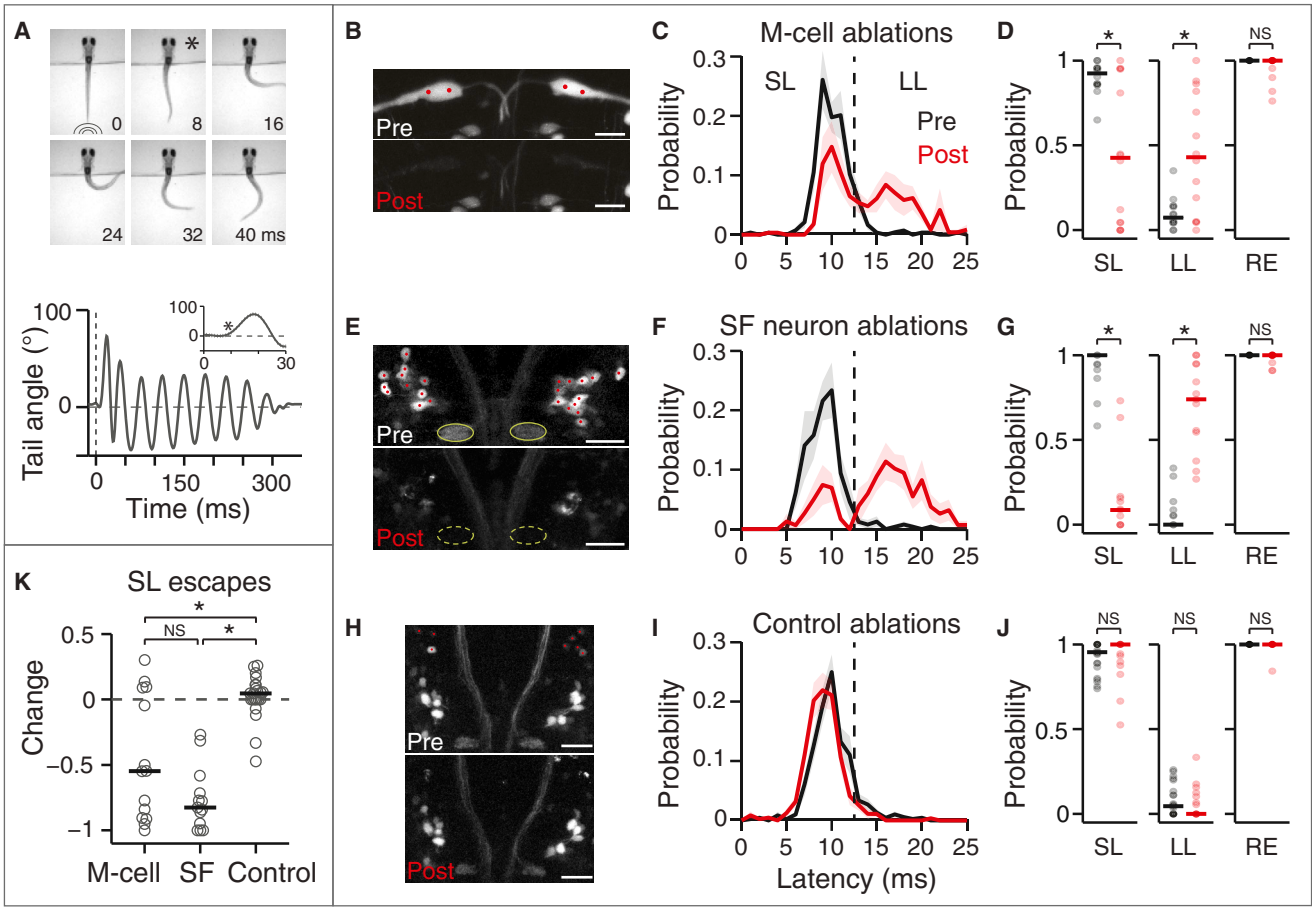

Figure 2. Loss of M-Cells or Spiral Fiber Neurons Largely Abolish Short-Latency Escapes

(A) Top: representative escape behavior of a head-embedded larval zebrafish responding to a tap stimulus. Images were recorded every millisecond, and here every eighth image is shown. The first image was taken at the time the tap stimulus hit the dish holding the larvae. The image marked with a star corresponds to the beginning of the escape response (8 ms latency). Bottom: representative smoothed tail trace showing the angle of the last tail segment with respect to the vertical in response to a tap. The escape behavior consists of a sharp-angle C-bend, followed by a counter turn in the opposite direction and subsequent swimming lasting hundreds of milliseconds. The dotted line shows the stimulus. The inset shows the first 300 ms after stimulus onset and the star indicates the start of the C-bend.

(B–J) Results of M-cell ablations (B–D; n = 14 fish), spiral fiber (SF) neuron ablations (E–G; n = 13), and control ablations (H–J; n = 23) on the escape behavior in response to taps.

(B, E, and H) Stack projections showing before (top) and immediately after (B) or 24 hr after (E and H) two-photon laser-mediated bilateral ablations (bottom). Shown are *Et(fos:Gal4-VP16)s1181t*; *Tg(UAS:GCaMP-HS)* (B) and *Tg(–6.7FRhcrtR:gal4VP16); Tg(UAS-E1b:Kaede)* (E and H). Red dots mark the cells or location within the M-cell that were targeted for ablation. Green ovals in (E) mark the axon caps, which are no longer apparent 24 hr after ablations. High-fluorescence cell debris can be observed in the post images.

(C, F, and I) Escape probability as a function of latency of all escapes performed, mean ± SEM, before (black) and after (red) ablations. The dotted line at 13 ms demarcates short-latency (≦12 ms) and long-latency (13–25 ms) escapes.

(D, G, and J) Probabilities of different types of responses as a function of all trials before (black) and after (red) ablations. Individual fish are displayed as semi-transparent dots, and horizontal bars are the medians. Left, SL escapes; middle, LL escapes; right, overall responses. M-cell: p = 0.013 pre versus post (SL), 0.016 (LL), and 0.125 (RE); spiral fiber neuron: $p = 2.4 \times 10^{-4}$, $p = 2.4 \times 10^{-4}$, and p = 0.25; control: p = 0.28, p = 0.20, and p = 1; Wilcoxon signed-rank test.

(K) Change in SL escape probability as a function of all trials (post – pre) based on the SL data plotted in (D), (G), and (J). Gray circles, individual fish; black line, median. M-cell versus spiral fiber neurons, p = 0.11; M-cell versus control, p = 0.011; spiral fiber neurons versus control, $p = 1.6 \times 10^{-6}$; Wilcoxon rank-sum test. *p < 0.05; NS, not significant. Pictures are oriented rostral up. Scale bars represent 20 μm. SF, spiral fiber; LS, short latency; LL, long latency; RE, overall response. See also Figure S2.

M-cell they project to (Figure 3F). The percentage of short-latency escapes contralateral to the ablated spiral fiber neuron somata increased from 44% ± 6.4% to 91% ± 4.1% (n = 17; Figure 3G), whereas the overall fast-escape escape probability remained unchanged (Figure 3D). The laterality bias after M-cell or spiral fiber neuron ablation was not statistically distinguishable (p > 0.05). These experiments support the requirement of spiral fiber neurons for the normal functioning of their target M-cell.

Spiral Fiber Neuron Activation Enhances the Probability of M-Cell-Mediated Escapes

Our results demonstrate that spiral fiber neurons are an essential excitatory input in the M-cell circuit. We next asked whether

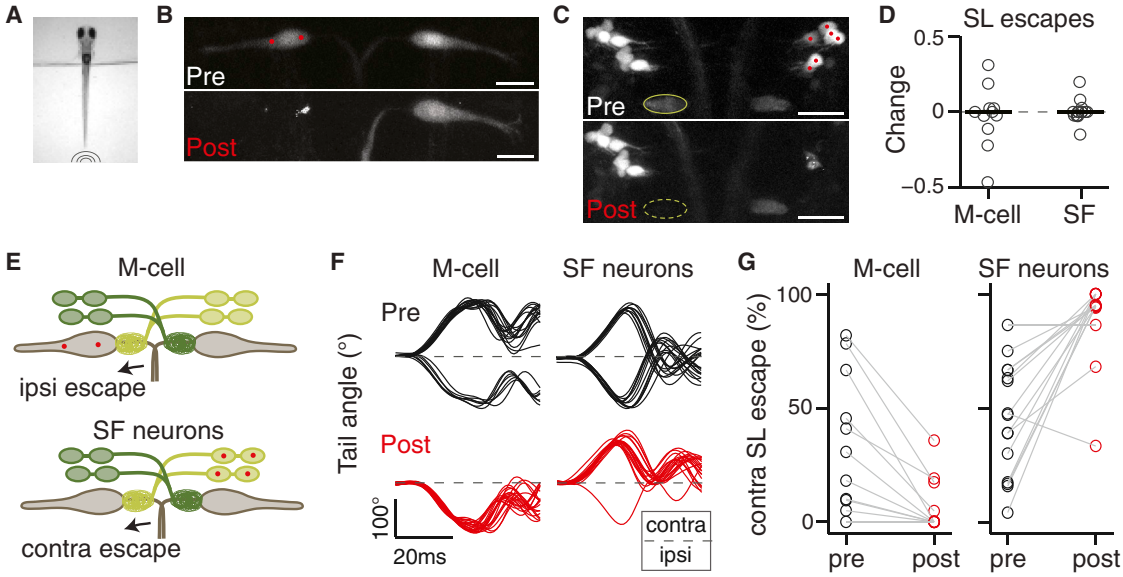

Figure 3. Spiral Fiber Neurons Are Necessary for Lateralized M-Cell-Mediated Escapes

(A) Tail-free larvae are presented with a non-directional tap stimulus as in Figure 2.

(B) Projection of two-photon image stack showing M-cells before (top) and 24 hr after (bottom) ablation of the M-cell on the left in *Et(fos:Gal4-VP16)s1181t; Tg(UAS-E1b:Kaede)*.

(C) Projection of two-photon image stack showing spiral fiber neurons before (top) and 24 hr after (bottom) ablation of spiral fiber neuron somata located on the right in *Tg(–6.7FRhcrtR:gal4VP16); Tg(UAS-E1b:Kaede)*. The axon cap (green oval) contralateral to the targeted spiral fiber neurons is no longer apparent 24 hr after ablations.

(D) Normalized change in short-latency (SL) escape probability as a function of all trials (post – pre). Gray circles, individual fish; black line, median. Left: M-cell ablation (n = 11). Right: spiral fiber neuron ablations (n = 17). The probability change is not significantly different from 0 in either condition (p = 0.67 and p = 0.98, respectively; Wilcoxon signed-rank test).

(E) Model showing that when M-cells or spiral fiber neurons are ablated unilaterally, escapes in response to taps become strongly biased toward one direction: ipsilateral to the ablated M-cell or contralateral to the ablated spiral fiber neurons.

(F) Example tail traces for a fish before (top plots; black) and after (bottom plots; red) ablation of the left M-cell (left plots) and a fish before and after ablations of spiral fiber neuron somata on the right (right plots). The directionality of the initial tail bend is expressed as ipsilateral or contralateral with respect to the ablated soma(ta). Traces begin at the time of tap delivery.

(G) Probability of contralateral SL escapes as a function of all SL escapes of either direction. Left: M-cell ablation. Right: spiral fiber neuron ablation. Escapes shift toward the ipsilateral side for M-cell ablation and to the contralateral side for spiral fiber neuron ablations. The laterality bias after M-cell or spiral fiber neuron ablation was not statistically distinguishable (p = 0.45, Wilcoxon rank-sum test).

Scale bars: 20 μm. Pictures are oriented rostral up. SF, spiral fiber; LS, short latency; contra, contralateral; ipsi, ipsilateral.

activating the spiral fiber neurons could decrease the threshold for M-cell-mediated escapes. To test this hypothesis, we used *Tg(14xUAS-E1b:hChR2(H134R)-EYFP)* to express channelrhodopsin2 (ChR2) in neurons labeled in *Tg(–6.7FRhcrtR:gal4VP16)*. We measured larval responsiveness to low-intensity taps alone or paired with blue light. ChR2 excitation light was delivered via a blue laser beam focused on the fish's head 20–60 ms before the tap occurred and for a total of 100 ms (Figure 4A). We observed a strong enhancement of short-latency, M-cell-mediated escapes in $ChR2^+$ fish when the weak taps were paired with blue light (4.4-fold enhancement; $p < 0.05$, Wilcoxon signed-rank test), but not in controls lacking ChR2 (Figure 4B). In addition to modulating the probability of short-latency escapes, we reasoned that the excitatory effect of spiral fiber neurons on the M-cell might decrease escape latency. Indeed, short-latency escapes in response to taps paired with light occurred on average 0.95 ms earlier than those in response to taps alone in $ChR2^+$ fish ($p < 0.05$). Latency was not affected in $ChR2^-$ controls (Figure 4C). The probability of long-latency escapes was also moderately enhanced by pairing taps with blue light in $ChR2^+$ fish only (2.1-fold mean increase), most likely due to unspecific ChR2-mediated effects. The latency of these escapes was not affected (Figures S3A and S3B).

To determine whether the ChR2-mediated enhancement of short-latency escapes was dependent on spiral fiber neurons, we tested behavior after spiral fiber neuron ablations. Short-latency escapes in response to taps alone were nearly abolished after spiral fiber neuron ablations, confirming our earlier ablation results. Crucially, pairing taps with blue light did not increase the probability of these escapes (Figure 4D). Our results suggest that spiral fiber neurons are necessary for the ChR2-mediated enhancement of M-cell-mediated escapes.

We next asked whether excitation of spiral fiber neurons alone could evoke escape behaviors. In half of the larvae (11/22), a 100-ms blue light pulse gave rise to escapes with a probability above 10% (Figure 4E). Spiral fiber neuron ablations eliminated these escapes in all but one larva, where lesions may have been incomplete. Optically induced escapes were kinematically similar to those induced by taps, but the angle of the initial C-bend was lower (Figures S3C and S3D), in agreement with

 ©2015 Elsevier Ltd All rights reserved

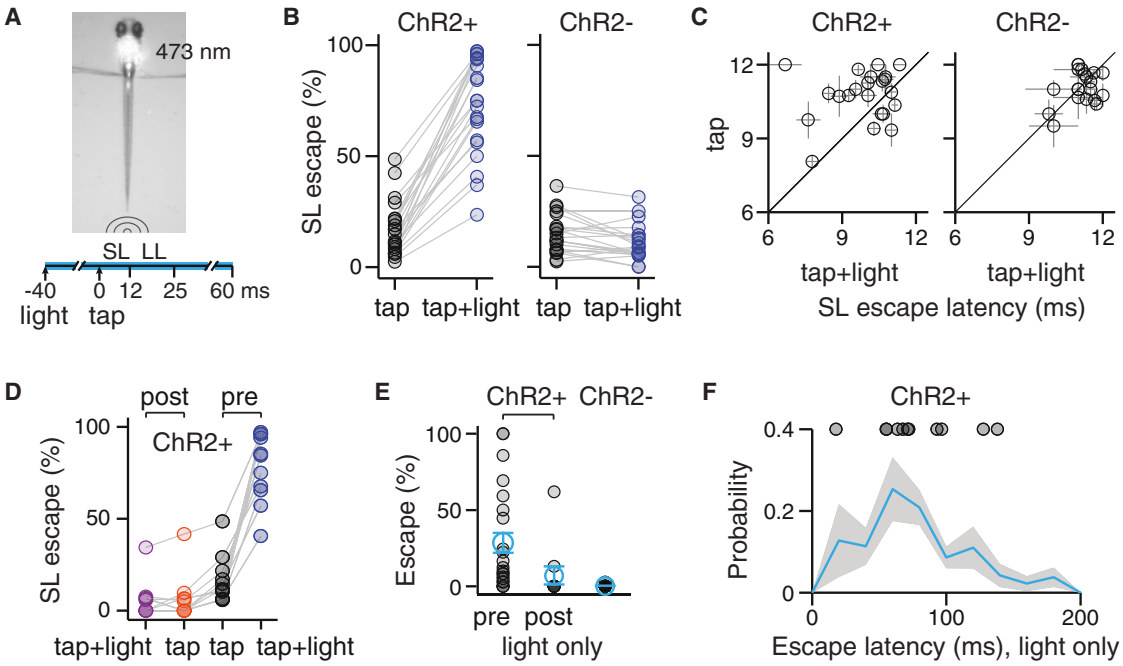

Figure 4. Activation of Spiral Fiber Neurons Enhances the Probability of M-Cell-Mediated Escapes

(A) 473-nm blue light is shone on the hindbrain of *Tg(–6.7FRhcrtR:gal4VP16); Tg(14xUAS-E1b:hChR2(H134R)-EYFP)* larvae using a focused laser beam for a total of 100 ms. 20–60 ms after the onset of the light, a low-intensity tap is delivered, and tail movements are scored for short-latency (SL) or long-latency (LL) escapes.

(B) Percentage of SL escapes for individual fish in response to taps alone (black circles) and taps paired with blue light (blue circles). Left: ChR2$^+$ fish (n = 22; 17% ± 4.9% tap, 73.4% ± 4.7% tap + light, mean ± SEM, corresponding to a 4.4-fold enhancement of SL escapes with blue light; $p = 4.0 \times 10^{-5}$). Right: ChR2$^-$ controls (n = 22; 15% ± 1.9% tap, 11% ± 1.7% tap + light, corresponding to a 1.4-fold decrease of SL escapes with blue light; p = 0.01, Wilcoxon signed-rank test).

(C) SL escape latency in milliseconds in response to taps (y axis) or taps paired with blue light (x axis) for individual fish tested (black circles). Left: ChR2$^+$ fish (n = 22; 11 ± 0.22 ms tap, 9.9 ± 0.27 ms tap + light, mean ± SEM; p = 0.01). Right: ChR2$^-$ fish (n = 22; 11 ± 0.14 ms tap, 11 ± 0.13 ms ms tap + light; p = 0.72, Wilcoxon signed-rank test).

(D) Percentage of SL escapes in response to taps or taps paired with light before (pre) or after (post) bilateral spiral fiber neuron ablations. (n = 11 ChR$^+$ larvae; pre: 17% ± 3.7% tap, 78 ± 5.4% tap + light, mean ± SEM, corresponding to a 4.7-fold enhancement; $p = 9.8 \times 10^{-4}$; post: 6.3% ± 3.5% tap, 5.6 ± 2.9% tap + light, p = 0.58; Wilcoxon signed-rank test). Data in the pre condition are a subset of the data in (B).

(E) Percentage of escapes for individual fish (black circles, mean ± SEM in blue) in response to blue light alone (in the absence of taps). ChR2$^+$ fish before (pre; n = 22) and after (post; n = 11) spiral fiber neuron ablations. ChR2$^-$ fish, n = 22.

(F) Distribution of escape latencies in ChR2$^+$ fish after the onset of a 100-ms blue light pulse (blue line ± shaded SEM; n = 185 escapes, n = 11 fish). Circles represent the mean of escape latencies for larvae displaying >10% probability of escapes (see "pre" in E; n = 11). Note: to ensure that escapes to blue light alone could be disambiguated with escapes in response to taps paired with light, larvae that responded to blue light alone with mean escapes latencies <70 ms were tested with a 20-ms delay between taps and blue light; otherwise, 40- or 60-ms delays were used (see A). See also the Supplemental Experimental Procedures. ChR2, channelrhodopsin 2; LS, short latency; LL, long latency. See also Figure S3.

reports that electrical stimulation of the M-cell alone gives rise to less effective escapes [24]. The latency from onset of blue light to behavior was long and variable (70 ± 30 ms, mean ± SD; Figure 4F), which is not unusual for ChR2-mediated behavior [25–27] (but see [28]). The effectiveness of blue light correlated with escape latencies across fish (Figures S3E–S3G) and most likely reflects ChR2 expression levels. Together, our optogenetic results indicate that exciting the spiral fiber neurons potentiates M-cell-mediated behavior.

DISCUSSION

Our study unveils a functional pathway by which sensory information is indirectly conveyed to the escape circuit: spiral fiber neurons respond to aversive cues and excite the M-cell at the axon cap. We provide three lines of evidence that support the notion that spiral fiber neurons are essential for M-cell-mediated escapes: (1) like M-cell ablations, bilateral spiral fiber neuron ablations nearly abolish short-latency escapes; (2) ablation of spiral fiber neurons unilaterally shifts the directionality of escapes; and (3) optical activation of spiral fiber neurons enhances M-cell-mediated escapes in response to subthreshold stimuli. In the following sections, we relate our data to previous electrophysiological studies of the M-cell, discuss the utility of a spatially and temporally distinct convergent pathway, and describe how convergent pathways may be an important motif in neural circuits.

Spiral Fiber Neuron Input Is Integrated with Dendritic Afferents at the M-Cell Axon Hillock

Previous electrophysiological recordings in the goldfish have identified an input of unknown origin onto the M-cell [29]. Our

findings suggest that this input has the characteristics of spiral fiber neuron excitation. In response to natural sounds, M-cell activity is composed of spatially and temporally distinct components: fast repetitive EPSPs are superimposed on an underlying slower depolarization [29]. Auditory/vestibular afferents making mixed electrical and chemical synapses on the M-cell lateral dendrites [30–32] are responsible for the fast component of the M-cell response and for part of the slower component [29]. The slower component also relies on an electrical and glutamatergic input near the soma [29], but the origin of this input is unknown. Spiral fiber neurons make both electrical and glutamatergic synapses close to the M-cell soma [9], and we find that they are active in response to sensory stimuli. This suggests that they are the origin of the secondary, slower component of the M-cell response, which was observed approximately 3 ms after the onset of the fast component. A 3-ms delay places this slower input within the M-cell's integration window: in response to auditory stimuli, initial depolarization in the goldfish M-cell occurs within 1 ms, but firing occurs from 3–12 ms [5, 33, 34]. Thus, in response to auditory/vibrational stimuli, excitatory inputs to the M-cell converge from two temporally and spatially distinct sources: distal sensory afferents provide rapid electrical and slower chemical input, and spiral fiber neurons provide a slow proximal input. Viral tracing experiments [35, 36] or other approaches are needed to identify the inputs of spiral fiber neurons.

To infer the site of integration of the dendritic and indirect inputs onto the M-cell, we recorded stimulus-elicited calcium activity in the M-cell soma before and after spiral fiber neuron ablations (Figure S4). We found that spiral fiber neuron ablations did not significantly affect calcium dynamics in the M-cell soma in response to taps, suggesting that dendritic inputs are responsible for the bulk of the somatic depolarization. Since spiral fiber neurons play a necessary role in M-cell-mediated motor output, these experiments argue that inputs from spiral fiber neurons and direct sensory afferents are integrated at the level of the M-cell axon hillock to elicit an escape response (see the Supplemental Results and Discussion associated with Figure S4). Electrophysiological recordings of the M-cell axon and soma and specific activation of spiral fiber neurons are needed to explicitly determine the nature of this spatiotemporal integration.

Spiral Fiber Neurons Represent a Convergent Input that Enhances Circuit Robustness

Short-latency escapes, which are triggered by a single firing event in the M-cell, are vital to avoid predation but should be restricted to legitimate threats. Therefore, the M-cell must be reliably activated when necessary and otherwise be appropriately gated. The robust activation of the M-cell is faced with three hurdles: first, due to a low input resistance, short time constant, and hyperpolarized membrane potential, the M-cell requires strong currents to reach firing threshold [37]; second, feed-forward interneurons inhibit the M-cell [38, 39]; and third, dendritic excitation is strongly attenuated by the time it reaches the soma due to passive cable properties (up to 4-fold in the adult goldfish M-cell [29]). By providing an excitatory drive directly at the axon hillock, the site of action potential generation [40], spiral fiber neurons solve the challenge of overcoming the M-cell's high activation barrier. An additional challenge in the circuit is to ensure that the M-cell is not activated by innocuous short-lived sounds. Spiral fiber neurons introduce a delay line that may prevent unnecessary firing of the M-cell: transient depolarization of the M-cell by dendritic afferents would end before the necessary spiral fiber neuron input arrives at the axon hillock, precluding integration of the two pathways and rendering brief sensory input ineffective. Thus, in the M-cell escape circuit, indirect proximal input provides a necessary excitatory drive undiminished by distance and can serve as a mechanism to filter noise. Experiments combining stimulation of the two pathways and recordings in the M-cell are needed to directly test these scenarios.

Indirect Excitatory Pathways as a Circuit Motif

The spiral fiber neuron input is the first example of a necessary indirect pathway in a startle circuit. A diverse set of other circuits present anatomical similarities, where multiple, sometimes temporally and spatially segregated excitatory pathways converge. The interaction of inputs in these networks is poised to enhance the controllability and flexibility of the system and may provide additional opportunities for modulation. A first example is the crayfish escape network, in which tactile afferents project to command neurons and also to excitatory interneurons that then feed forward to the command neurons. The amplitude of excitation elicited by the interneurons is larger than the excitation coming from direct tactile afferents [41], suggesting that like spiral fiber neurons in the M-cell circuit, these crayfish interneurons might be essential for producing escapes. Another example is the mammalian hippocampus where CA1 pyramidal neurons receive sensory information via a direct and an indirect pathway. One path projects monosynaptically onto the neurons' distal dendrites but has a weak influence over somatic voltage. A slower trisynaptic pathway projecting to the proximal dendrites provides a stronger input [42]. Thus, similarly to spiral fiber neuron inputs in the M-cell circuit, the indirect pathway to CA1 introduces a powerful delay line that is more proximal. These examples of comparable circuitry in invertebrates and mammals suggest that the necessity of convergent excitatory pathways might be a general motif of neural circuits.

SUPPLEMENTAL INFORMATION

Supplemental Information includes Supplemental Results and Discussion, Supplemental Experimental Procedures, four figures, and one movie and can be found with this article online at http://dx.doi.org/10.1016/j.cub.2015.04.025.

AUTHOR CONTRIBUTIONS

A.M.B.L., D.S. and A.F.S. conceived the study. D.S. generated the *Tg(–6.7FRhcrtR:gal4VP16)* line. A.M.B.L. collected the data. A.M.B.L. analyzed the data with the guidance of D.S. and discussions with all authors. A.M.B.L. built the behavioral and ChR2 apparatus with help from D.N.R., D.S., M.H., C.L.W., and R.P. and wrote the software with D.N.R. and M.H. D.N.R. and J.M.L. built the two-photon calcium imaging apparatus. O.R. generated Movie S1. A.M.B.L. and A.F.S. wrote the manuscript with contributions from D.S., M.H., R.P., O.R., and F.E.

ACKNOWLEDGMENTS

We thank Adam Douglass and Jared Wortzman for generating the *Tg(UAS:GCaMP5)* fish; Koichi Kawakami for the *Tg(UAS:GCaMP-HS)* line; Herwig Baier for the *Et(fos:Gal4-VP16)s1181t* line; Joel Greenwood and Edward Soucy for technical support with the behavioral apparatus; Steve Zimmerman, Karen

 ©2015 Elsevier Ltd All rights reserved

Hurley, and Jessica Miller for fish care; and Misha Ahrens, Elizabeth Carroll, Timothy Dunn, Joseph Fetcho, Minoru Koyama, Florian Merkle, Iris Odstril, Yu-chin Pan, Carlos Pantoja, Constance Richter, Kristen Severi, and additional members of the F.E. and A.F.S. labs for many helpful discussions. A.M.B.L. was supported by a Theodore H. Ashford Graduate Fellowship in the Sciences, an NSF Graduate Research Fellowship, and NIH T32HL007901. D.S. was supported by a Helen Hay Whitney Postdoctoral Fellowship and NIDCD K99DC012775. M.H. was supported by an EMBO Long-Term Postdoctoral Fellowship (ALTF 1056-10) and a postdoctoral fellowship by the Jane Coffin Childs Fund for Biomedical Research. O.R. was supported by an HFSP Long-Term Fellowship (LT000772/2012). C.L.W. was supported by the Agency for Science, Technology and Research, Singapore. Research was supported by NIH grant R01HL109525 awarded to A.F.S.

Received: June 17, 2014
Revised: March 9, 2015
Accepted: April 14, 2015
Published: May 7, 2015

REFERENCES

1. Zottoli, S.J., and Faber, D.S. (2000). The Mauthner cell: what has it taught us? Neuroscientist *6*, 26–38.
2. Eaton, R.C., Lee, R.K., and Foreman, M.B. (2001). The Mauthner cell and other identified neurons of the brainstem escape network of fish. Prog. Neurobiol. *63*, 467–485.
3. Korn, H., and Faber, D.S. (2005). The Mauthner cell half a century later: a neurobiological model for decision-making? Neuron *47*, 13–28.
4. Pfaff, D.W., Martin, E.M., and Faber, D. (2012). Origins of arousal: roles for medullary reticular neurons. Trends Neurosci. *35*, 468–476.
5. Zottoli, S.J. (1977). Correlation of the startle reflex and Mauthner cell auditory responses in unrestrained goldfish. J. Exp. Biol. *66*, 243–254.
6. Liu, K.S., and Fetcho, J.R. (1999). Laser ablations reveal functional relationships of segmental hindbrain neurons in zebrafish. Neuron *23*, 325–335.
7. Kohashi, T., and Oda, Y. (2008). Initiation of Mauthner- or non-Mauthner-mediated fast escape evoked by different modes of sensory input. J. Neurosci. *28*, 10641–10653.
8. Burgess, H.A., and Granato, M. (2007). Sensorimotor gating in larval zebrafish. J. Neurosci. *27*, 4984–4994.
9. Koyama, M., Kinkhabwala, A., Satou, C., Higashijima, S., and Fetcho, J. (2011). Mapping a sensory-motor network onto a structural and functional ground plan in the hindbrain. Proc. Natl. Acad. Sci. USA *108*, 1170–1175.
10. Kimmel, C.B., Sessions, S.K., and Kimmel, R.J. (1981). Morphogenesis and synaptogenesis of the zebrafish Mauthner neuron. J. Comp. Neurol. *198*, 101–120.
11. Scott, J.W., Zottoli, S.J., Beatty, N.P., and Korn, H. (1994). Origin and function of spiral fibers projecting to the goldfish Mauthner cell. J. Comp. Neurol. *339*, 76–90.
12. Lorent, K., Liu, K.S., Fetcho, J.R., and Granato, M. (2001). The zebrafish space cadet gene controls axonal pathfinding of neurons that modulate fast turning movements. Development *128*, 2131–2142.
13. Gyda, M., Wolman, M., Lorent, K., and Granato, M. (2012). The tumor suppressor gene retinoblastoma-1 is required for retinotectal development and visual function in zebrafish. PLoS Genet. *8*, e1003106.
14. Muto, A., Ohkura, M., Kotani, T., Higashijima, S., Nakai, J., and Kawakami, K. (2011). Genetic visualization with an improved GCaMP calcium indicator reveals spatiotemporal activation of the spinal motor neurons in zebrafish. Proc. Natl. Acad. Sci. USA *108*, 5425–5430.
15. O'Malley, D.M., Kao, Y.-H., and Fetcho, J.R. (1996). Imaging the functional organization of zebrafish hindbrain segments during escape behaviors. Neuron *17*, 1145–1155.
16. Ikeda, H., Delargy, A.H., Yokogawa, T., Urban, J.M., Burgess, H.A., and Ono, F. (2013). Intrinsic properties of larval zebrafish neurons in ethanol. PLoS ONE *8*, e63318.
17. Ernest, S., Rauch, G.J., Haffter, P., Geisler, R., Petit, C., and Nicolson, T. (2000). Mariner is defective in myosin VIIA: a zebrafish model for human hereditary deafness. Hum. Mol. Genet. *9*, 2189–2196.
18. Harris, J.A., Cheng, A.G., Cunningham, L.L., MacDonald, G., Raible, D.W., and Rubel, E.W. (2003). Neomycin-induced hair cell death and rapid regeneration in the lateral line of zebrafish (Danio rerio). J. Assoc. Res. Otolaryngol. *4*, 219–234.
19. Bianco, I.H., Ma, L.-H., Schoppik, D., Robson, D.N., Orger, M.B., Beck, J.C., Li, J.M., Schier, A.F., Engert, F., and Baker, R. (2012). The tangential nucleus controls a gravito-inertial vestibulo-ocular reflex. Curr. Biol. *22*, 1285–1295.
20. Kohashi, T., Nakata, N., and Oda, Y. (2012). Effective sensory modality activating an escape triggering neuron switches during early development in zebrafish. J. Neurosci. *32*, 5810–5820.
21. Issa, F.A., O'Brien, G., Kettunen, P., Sagasti, A., Glanzman, D.L., and Papazian, D.M. (2011). Neural circuit activity in freely behaving zebrafish (Danio rerio). J. Exp. Biol. *214*, 1028–1038.
22. Satou, C., Kimura, Y., Kohashi, T., Horikawa, K., Takeda, H., Oda, Y., and Higashijima, S. (2009). Functional role of a specialized class of spinal commissural inhibitory neurons during fast escapes in zebrafish. J. Neurosci. *29*, 6780–6793.
23. Takahashi, M., Narushima, M., and Oda, Y. (2002). In vivo imaging of functional inhibitory networks on the mauthner cell of larval zebrafish. J. Neurosci. *22*, 3929–3938.
24. Nissanov, J., Eaton, R.C., and DiDomenico, R. (1990). The motor output of the Mauthner cell, a reticulospinal command neuron. Brain Res. *517*, 88–98.
25. Douglass, A.D., Kraves, S., Deisseroth, K., Schier, A.F., and Engert, F. (2008). Escape behavior elicited by single, channelrhodopsin-2-evoked spikes in zebrafish somatosensory neurons. Curr. Biol. *18*, 1133–1137.
26. Kubo, F., Hablitzel, B., Dal Maschio, M., Driever, W., Baier, H., and Arrenberg, A.B. (2014). Functional architecture of an optic flow-responsive area that drives horizontal eye movements in zebrafish. Neuron *81*, 1344–1359.
27. Thiele, T.R., Donovan, J.C., and Baier, H. (2014). Descending control of swim posture by a midbrain nucleus in zebrafish. Neuron *83*, 679–691.
28. Monesson-Olson, B.D., Browning-Kamins, J., Aziz-Bose, R., Kreines, F., and Trapani, J.G. (2014). Optical stimulation of zebrafish hair cells expressing channelrhodopsin-2. PLoS ONE *9*, e96641.
29. Szabo, T.M., Weiss, S.A., Faber, D.S., and Preuss, T. (2006). Representation of auditory signals in the M-cell: role of electrical synapses. J. Neurophysiol. *95*, 2617–2629.
30. Nakajima, Y. (1974). Fine structure of the synaptic endings on the Mauthner cell of the goldfish. J. Comp. Neurol. *156*, 379–402.
31. Tuttle, R., Masuko, S., and Nakajima, Y. (1986). Freeze-fracture study of the large myelinated club ending synapse on the goldfish Mauthner cell: special reference to the quantitative analysis of gap junctions. J. Comp. Neurol. *246*, 202–211.
32. Lin, J.W., and Faber, D.S. (1988). Synaptic transmission mediated by single club endings on the goldfish Mauthner cell. I. Characteristics of electrotonic and chemical postsynaptic potentials. J. Neurosci. *8*, 1302–1312.
33. Eaton, R., and Lavender, W. (1981). Identification of Mauthner-initiated response patterns in goldfish: evidence from simultaneous cinematography and electrophysiology. J. Comp. Physiol. *144*, 521–531.
34. Weiss, S.A., Zottoli, S.J., Do, S.C., Faber, D.S., and Preuss, T. (2006). Correlation of C-start behaviors with neural activity recorded from the hindbrain in free-swimming goldfish (Carassius auratus). J. Exp. Biol. *209*, 4788–4801.
35. Zhu, P., Narita, Y., Bundschuh, S.T., Fajardo, O., Schärer, Y.P., Chattopadhyaya, B., Bouldoires, E.A., Stepien, A.E., Deisseroth, K., Arber, S., et al. (2009). Optogenetic dissection of neuronal circuits in zebrafish using viral gene transfer and the Tet system. Front Neural Circuits *3*, 21.

36. Mundell, N.A., Beier, K.T., Pan, Y.A., Lapan, S.W., Göz Aytürk, D., Berezovskii, V.K., Wark, A.R., Drokhlyansky, E., Bielecki, J., Born, R.T., et al. (2015). Vesicular stomatitis virus enables gene transfer and transsynaptic tracing in a wide range of organisms. J. Comp. Neurol. Published online February 17, 2015. http://dx.doi.org/10.1002/cne.23761.

37. Curti, S., and Pereda, A.E. (2010). Functional specializations of primary auditory afferents on the Mauthner cells: interactions between membrane and synaptic properties. J. Physiol. Paris *104*, 203–214.

38. Zottoli, S.J., and Faber, D.S. (1980). An identifiable class of statoacoustic interneurons with bilateral projections in the goldfish medulla. Neuroscience *5*, 1287–1302.

39. Faber, D.S., Fetcho, J.R., and Korn, H. (1989). Neuronal networks underlying the escape response in goldfish. General implications for motor control. Ann. N Y Acad. Sci. *563*, 11–33.

40. Furshpan, E.J., and Furukawa, T. (1962). Intracellular and extracellular responses of the several regions of the Mauthner cell of the goldfish. J. Neurophysiol. *25*, 732–771.

41. Zucker, R.S. (1972). Crayfish escape behavior and central synapses. I. Neural circuit exciting lateral giant fiber. J. Neurophysiol. *35*, 599–620.

42. Dudman, J.T., Tsay, D., and Siegelbaum, S.A. (2007). A role for synaptic inputs at distal dendrites: instructive signals for hippocampal long-term plasticity. Neuron *56*, 866–879.

 ©2015 Elsevier Ltd All rights reserved

Current Biology

Supplemental Information

A Convergent and Essential Interneuron Pathway for Mauthner-Cell-Mediated Escapes

Alix M.B. Lacoste, David Schoppik, Drew N. Robson, Martin Haesemeyer, Ruben Portugues, Jennifer M.B. Li, Owen Randlett, Caroline L. Wee, Florian Engert, and Alexander F. Schier

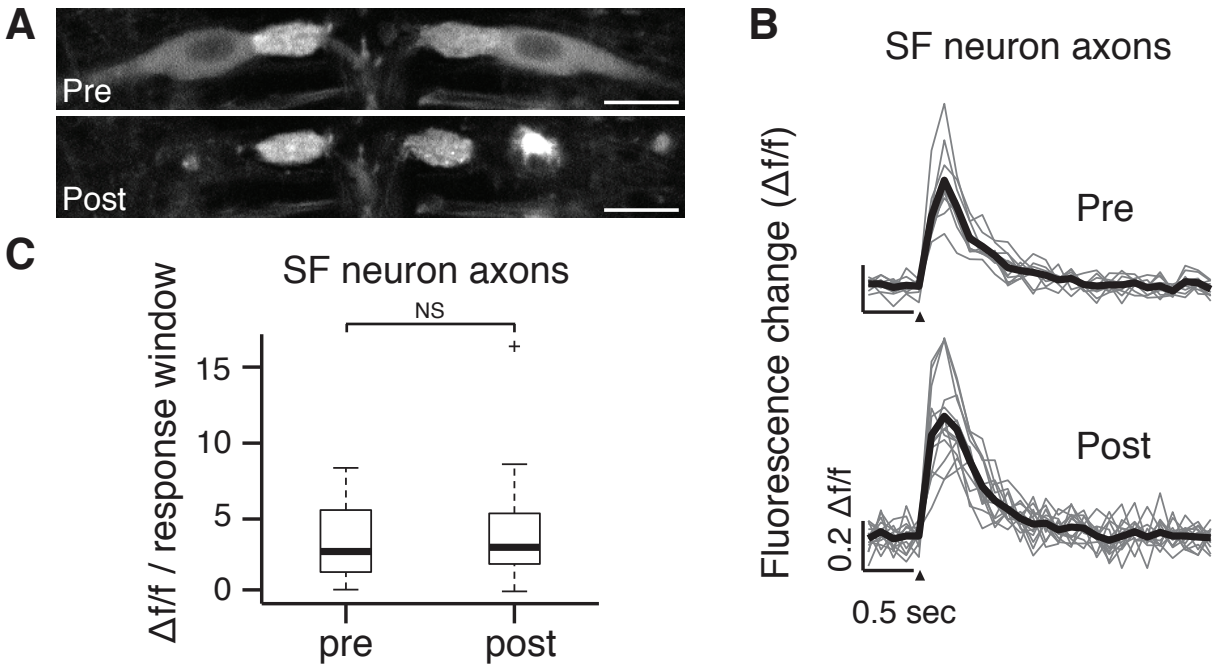

Figure S1, related to Figure 1. Spiral fiber neuron axons continue to respond to taps after M-cell ablations.

(A) Two-photon image showing M-cells and spiral fiber neuron axon terminals at the axon cap in *Tg(-6.7FRhcrtR:gal4VP16)* ; *Et(fos:Gal4-VP16)s1181t* ; *Tg(UAS:GCaMP5)* before (top image) and after (bottom image) bilateral ablation of the M-cells. Bright spots in the bottom image correspond to cell debris. Scale bar: 20 μm. Pictures are oriented rostral up.

(B) Representative traces of the change in spiral fiber (SF) neuron axon fluorescence at the M-cell axon cap in response to taps. Top plot: before, bottom plot: after bilateral ablation of the M-cells. Grey traces are individual trials, the black trace is the mean. Stimulus delivery is indicated by an arrowhead.

(C) Population fluorescence change of spiral fiber (SF) neuron axons in response to taps before (left) and after (right) ablation of the M-cells (n = 10 axon caps, y-axis is the mean fluorescence change over a 1.5 sec response window in trials where the axon cap responded). Horizontal line is the median, box edges are the 25th and 75th percentiles, whiskers extend to the most extreme data points not considered outliers and crosses are outliers. Pre and post are not significantly different (NS, p = 1, Wilcoxon signed rank sum test).

Abbreviation: SF: spiral fiber.

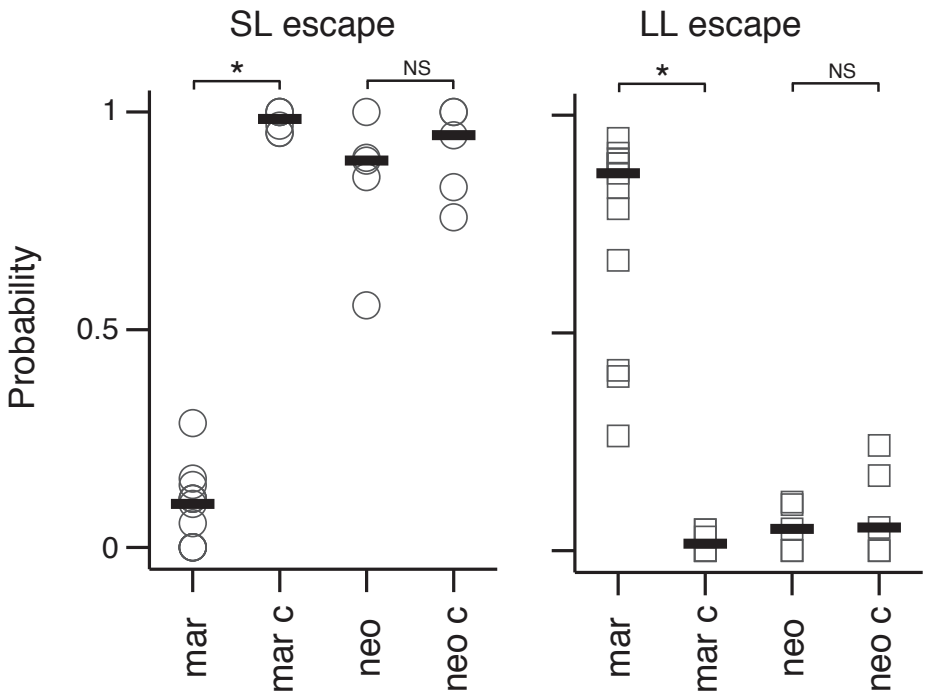

Figure S2, related to Figure 2. Short-latency escapes in response to taps are mediated by the inner ear.

Probability of generating escapes in response to taps in the tail-free behavioral apparatus. Fish tested are homozygote *mariner* mutant fish lacking mechanosensory transduction in hair cells (mar, n = 13) and wild-type or heterozygote siblings (mar c, n = 6); neomycin-treated fish with ablated lateral lines (neo, n = 5) and control siblings (neo c, n = 5). Left panel: short-latency (SL) escapes. Right panel: long-latency (LL) escapes. Mariner mutants are significantly different from their controls ($p = 7.4*10^{-5}$ and $7.4*10^{-5}$ for SL and LL escapes respectively) whereas neomycin treated fish and their controls are not ($p = 0.69$ and 0.65). * denotes $p < 0.05$ by Wilcoxon rank sum test.

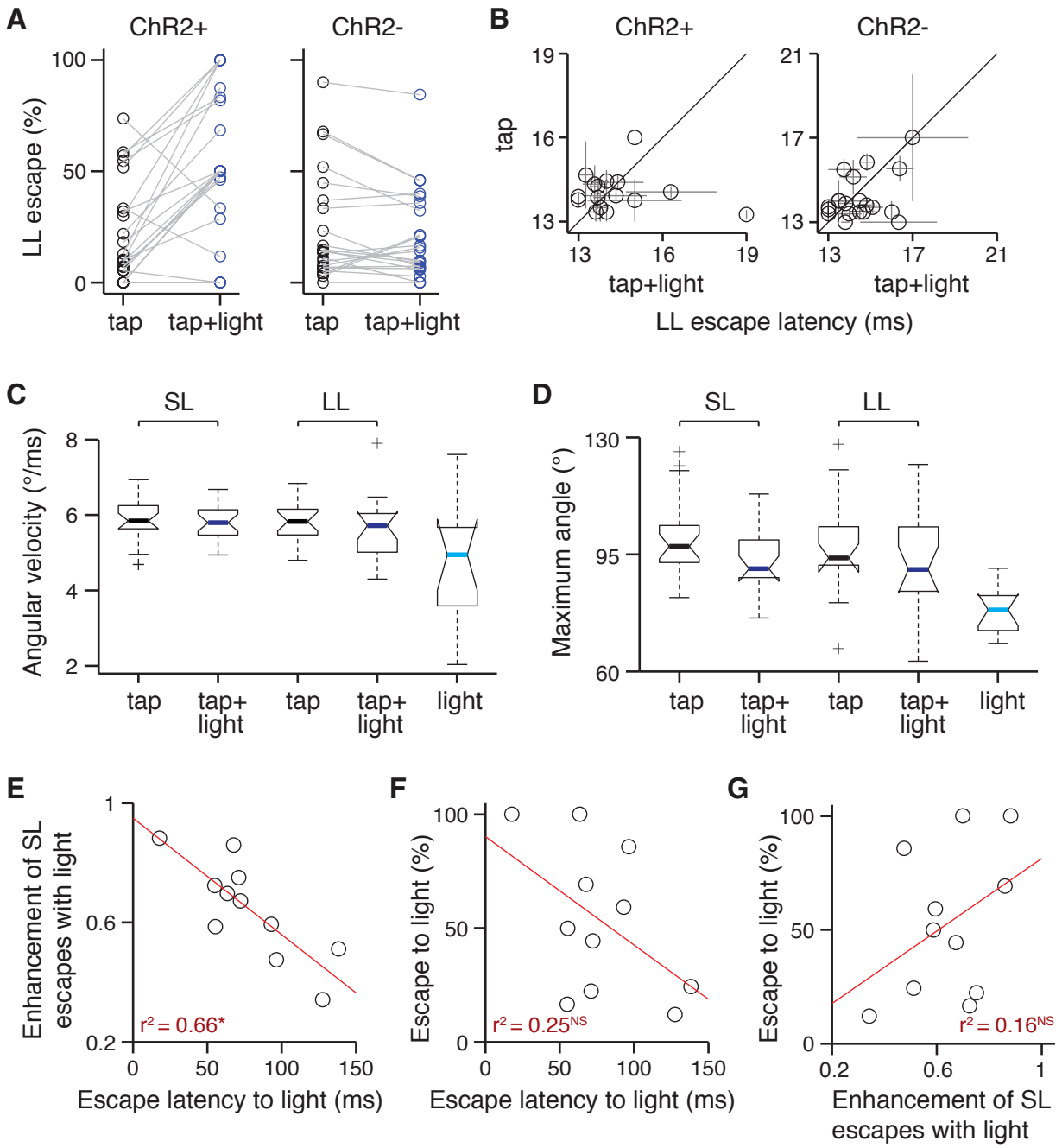

Figure S3, related to Figure 4. Characteristics of escapes with optogenetic activation of spiral fiber neurons.

(A) % Long-latency (LL) escapes for individual fish in response to taps alone (black circles) and taps paired with blue light (blue circles). Left panel: ChR2+ fish (n = 22, 23% ± 4.9% tap, 54% ± 7.1% tap + light, mean ± SEM, corresponding to a 2.4 fold enhancement of LL escapes with blue light, $p = 6.8*10^{-4}$). Part of this enhancement could be due to the blue light alone eliciting

escapes. Right panel: ChR2- controls (n = 22, 25% ± 5.3% tap, 21% ± 4.4% tap + light, p = 0.12, Wilcoxon signed rank test).

(B) LL escape latency in ms in response to taps (y-axis) or taps paired with blue light (x-axis). Left panel: ChR2+ fish (n = 22, 14.4 ms ± 0.41 ms tap, 14.3 ms ± 0.30 ms tap + light, mean ± SEM, p = 0.57). Right panel: ChR2- fish (n = 22, 14.1 ms ± 0.23 ms tap, 14.5 ms ± 0.25 ms tap + light, p = 0.27).

(C) Mean angular velocity of the initial C-bend in SL or LL escapes in response to taps, taps paired with blue light in ChR2+ larvae (n = 22), or blue light alone in ChR2+ larvae whose response probability to light alone exceeded 10% (n = 11). Horizontal lines are the medians across fish, box edges are the 25th and 75th percentiles, whiskers extend to the most extreme data points not considered outliers, box plots whose notches do not overlap have different medians at the 5% significance level, and crosses are outliers. The light condition is significantly different from the other 4 conditions. Other comparisons are not significant (multiple comparisons test after ANOVA, α = 0.05).

(D) Mean maximum angle of the initial C-bend in SL or LL escapes in response to taps, taps paired with blue light in ChR2+ larvae (n = 22), or blue light alone in ChR2+ larvae whose response probability to light alone exceeded 10% (n = 11). The light condition is significantly different from the other 4 conditions. Other comparisons are not significant.

(E–G) Correlation between escape latency in response to blue light, enhancement in the probability of SL escapes when taps are paired with blue light (probability of SL escapes to tap+light - probability of SL escapes to tap), and probability of escapes to blue light. ChR2+ larvae whose response probability to light alone exceeded 10% are represented as circles (11/22 tested). r^2 values represent the goodness of fit from linear regression (red line). * denotes $p < 0.05$; NS: $p > 0.05$ comparing F-statistics and constant model.

Abbreviations: ChR2: channelrhodopsin 2; LS: short-latency; LL: long-latency.

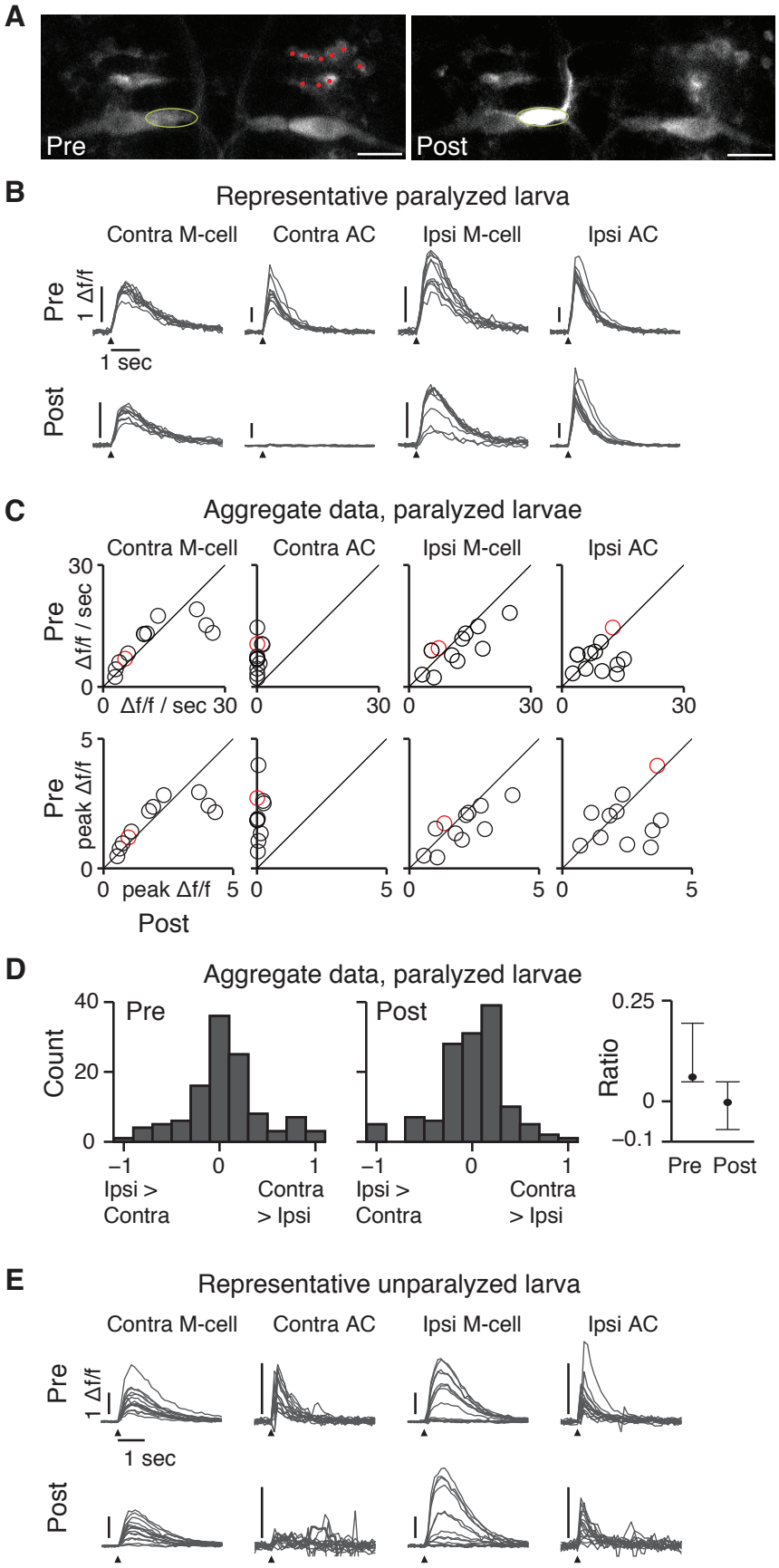
A
Pre
Post
B
Representative paralyzed larva
Contra M-cell
Contra AC
Ipsi M-cell
Ipsi AC
Pre
1 Δf/f
1 sec
Post
C
Aggregate data, paralyzed larvae
Contra M-cell
Contra AC
Ipsi M-cell
Ipsi AC
Pre
Δf/f / sec
0 Δf/f / sec 30
0
30
peak Δf/f
0 peak Δf/f 5
5
Post
D
Aggregate data, paralyzed larvae
Pre
Post
Count
40
20
0
−1
0
1
Ipsi > Contra
Contra > Ipsi
Ratio
0.25
0
−0.1
Pre
Post
E
Representative unparalyzed larva
Contra M-cell
Contra AC
Ipsi M-cell
Ipsi AC
Pre
1 Δf/f
1 sec
Post

Figure S4, related to Discussion. Spiral fiber neuron ablations do not change somatic M-cell calcium dynamics in response to taps.

(A) Projection of two-photon image stack showing M-cells and spiral fiber neurons in *Tg(-6.7FRhcrtR:gal4VP16)* ; *Et(fos:Gal4-VP16)s1181t* ; *Tg(UAS:GCaMP5)* (projection). Top: before ablation of spiral fiber neurons on the right (red dots). Bottom: immediately after ablations. The left axon cap corresponding to spiral fiber neuron axons (green oval) fluoresces strongly due to calcium release upon ablations. Scale bar: 20 µm. Pictures are oriented rostral up.

(B) Change in fluorescence (Δf/f) in response to taps (arrowheads) before and after unilateral spiral fiber neuron ablations for one representative fish paralyzed with alpha-bungarotoxin and embedded in agarose. Contra M-cell: M-cell located contralateral to the ablated spiral fiber neuron somata; Contra AC: contralateral axon cap corresponding to axon terminals of the ablated spiral fiber neurons; Ipsi M-cell: ipsilateral M-cell with preserved spiral fiber neuron input; Ipsi AC: axon cap corresponding to axon terminals of the intact spiral fiber neurons. The mean across trials is plotted in black and individual trials in grey. Top panels: before unilateral spiral fiber neuron ablations; bottom panels: after spiral fiber neuron ablations. Stimulus delivery is indicated by an arrowhead.

(C) Mean response amplitude in individual larvae (circles), before and after unilateral spiral fiber neuron ablations. First row: values represent the mean Δf/f / sec, which was computed over a 1.5 sec response window across trials with a non-zero Δf/f. The median difference pre versus post was statistically significant only in the contralateral axon cap (Contra M-cell, $p = 0.90$; Contra AC, $p = 9.8*10^{-4}$; Ipsi M-cell, $p = 0.067$; Ipsi AC, $p = 0.46$, Wilcoxon signed rank test, n = 11 fish). Second row: values represent the mean peak Δf/f across all trials. The median difference pre versus post was statistically significant only in the contralateral axon cap (Contra M-cell, $p = 0.90$; Contra AC, $p = 9.8*10-4$; Ipsi M-cell, $p = 0.083$; Ipsi AC, $p = 0.46$). The identity line is in black and the red circle represents the fish exemplified in B.

(D) Histograms showing the distribution of activity ratios between the ipsilateral and the contralateral M-cell before and after unilateral spiral fiber neuron ablations (ratio of response amplitudes normalized from -1 to 1: (contra - ipsi) / (contra + ipsi), Δf/f / sec, discarding trials in which both M-cell responses were flat, n = 130 trials pre and 139 trials post, across 11 larvae). Third panel: Histogram mean and 95% confidence interval (0.12, [0.010, 0.22], pre; 0, [-0.11, 0.11], post; $p = 0.18$, Wilcoxon rank sum test).

(E) Same as in B. except data is from a representative larva that was not paralyzed. Responses of the M-cells are graded and not affected by spiral fiber neuron ablations, similarly to responses in paralyzed fish.

Abbreviations: Contra: contralateral; Ipsi: ipsilateral; AC: spiral fiber neuron axon terminals at the axon cap.

SUPPLEMENTAL RESULTS AND DISCUSSION ASSOCIATED WITH FIGURE S4

Results. Spiral fiber neuron ablations do not change calcium dynamics in the M-cell soma in response to taps.

In response to auditory/vibrational stimuli, the M-cell receives two spatially segregated inputs, sensory afferents synapsing onto its dendrites, and spiral fiber neurons projecting to its axon hillock. An interesting question is where on the subcellular structure of the M-cell these two pathways converge. To test the effect of spiral fiber neuron input onto the M-cell, we analyzed M-cell calcium dynamics in response to taps before and after unilateral ablations of spiral fiber neurons (Figure S4A). Calcium signals could only be observed in the M-cell soma and not at the axon or axon hillock when spiral fiber neurons were not labeled. Therefore, unilateral spiral fiber neuron ablations allowed us to compare the M-cell soma lacking spiral fiber neuron projections with the other M-cell that retained spiral fiber neuron input, in the same animal.

We found that after unilateral spiral fiber neuron ablation, contralateral axon terminals failed to respond to taps, confirming the death of their associated somata (Figures S4B and S4C). M-cell and spiral fiber neuron axons ipsilateral to the ablated spiral fiber neuron somata continued to respond to stimuli with comparable fluorescence changes ($p > 0.05$, Wilcoxon signed rank test, Figures S4B and S4C). Contralateral M-cells that had lost spiral fiber neuron input also continued to respond to stimuli, and response amplitudes were comparable to the levels before spiral fiber neuron ablations ($p > 0.05$, Figure S4B). Comparing the relative amplitude of responses in the contralateral vs. ipsilateral M-cell, we found that this ratio did not change significantly after spiral fiber neuron ablations (Figure S4D). Our results were similar whether or not the larvae were paralyzed using alpha-bungarotoxin (Figure S4E). These results indicate that dendritic inputs are responsible for the bulk of calcium signals in the M-cell soma.

Discussion. Direct and feedforward excitatory inputs are integrated at the M-cell axon hillock.

The combined anatomical ([S1, S2]; Figure 1), electrophysiological ([S2, S3]), ablation (Figures 2 and 3), optogenetic (Figure 4), and calcium imaging (Figure S4) data support a model wherein spiral fiber neuron and afferent inputs are integrated at the level of the M-cell axon hillock. Others have found that large amplitude calcium activity in the M-cell is correlated with short-latency escapes, and similar to calcium activity elicited by antidromic action potentials [S4]. Our

results suggest that without spiral fiber neuron input, the M-cell's ability to fire is compromised. One might ask, then, why the loss of spiral fiber neuron input did not decrease calcium levels in the M-cell soma. Differences between our study and published reports may explain this apparent inconsistency. First, while others mainly observe all or none calcium events in the M-cells that are thought to indicate firing events [S4-S7], our recordings show graded responses (Figures S4B, S4D and S4E). This difference may be due to the type of calcium indicator or the type of stimulus used. Second, studies using unilateral stimuli report that only one M-cell is active at a time [S4, S5, S7]. In contrast, we observe concurrent activity in the M-cells (Figure S4D). This is consistent with a study by Satou and colleagues [S6] who find that the M-cells were coactive 55% of the time in response to non-directional stimuli. Their data suggest that in these cases, both M-cells fire, but with a delay, and that the excitatory effects of the trailing spikes are shunted by commissural inhibitory neurons in the spinal cord. However, the authors observe a higher probability of co-activity in the M-cells by calcium imaging compared to what was inferred from behavioral analysis (55% vs. 30%). Therefore, the calcium transients observed may not be accurate predictors of action potentials. Instead, they may primarily reflect sensory input rather than output. It is conceivable that the strong excitatory drive generated by auditory/vestibular afferents can saturate the slow-kinetic calcium indicator in the M-cell soma, and mask the potential effect of backpropagating depolarization. In our ablation experiments, direct sensory input is intact and may dominate measurable somatic calcium entry in the M-cell. Thus, our results imply that dendritic afferents elicit the bulk of calcium entry into the M-cell soma and that spiral fiber neuron actions are primarily restricted to the axon hillock. Since M-cell mediated behavior is impaired in the absence of spiral fiber neurons, it suggests spiral fiber neuron and dendritic inputs are integrated not in the M-cell soma but rather at the level of the M-cell axon hillock, the site of action potential initiation [S8].

SUPPLEMENTAL EXPERIMENTAL PROCEDURES

Zebrafish care and strains

All protocols and procedures involving zebrafish were approved by the Harvard University/Faculty of Arts & Sciences Standing Committee on the Use of Animals in Research and Teaching (IACUC). Larvae were raised at 28.5°C on a standard 14/10 hour light/dark cycle at a density of 20-50 fish in 10 cm diameter petri dishes filled with 25-40 mL buffered E3 (1mM HEPES added). *Mitfa-/-* mutants that lack melanophores were used for all ablation and calcium imaging experiments.

Generation of transgenic fish

Tg(-6.7FRhcrtR:gal4VP16): -6.7FRhcrtR was amplified using a nested PCR strategy. First, a 6775bp DNA fragment immediately upstream of the *Fugu rubripes hcrtr2* start site was amplified from genomic DNA, using a high-fidelity polymerase (PfuUltra II Fusion, Stratagene) with primers 5'-AATCCAAATTCCCAGTGACG-3' and 5'- CCAGATACTCGGCAAACAAA-3', 56° C annealing temperature, 1:45 elongation time. The PCR product was TOPO cloned into a TA vector (Life Technologies). Using the resulting plasmid as a template, a 6732bp fragment was amplified using primers 5'- AATCCAAATTCCCAGTGACG-3' and 5'-CCAGATACTCGGCAAACAAA-3', 55°C annealing temperature, 1:45 elongation and similarly TOPO cloned into a GATEWAY-compatible vector (PCR8/GW, Life Technologies). The resulting entry vector was recombined into a destination vector upstream of gal4-VP16, between Tol2 integration arms [S9]. *Tg(UAS-E1b:Kaede)s1999t* [S10] embryos were injected at the one-cell stage with 0.5nL of 50ng/uL plasmid and 35ng/uL *Tol2 transposase* mRNA in water, and their progeny screened for fluorescence. One founder produced three fluorescent progeny; one survived. To identify transgenic fish without using a UAS reporter, potential carriers were genotyped using the following primers to generate a 592bp product spanning the upstream Tol2 arm and the start of the *Fugu* sequence: 5'- CAATCCTGCAGTGCTGAAAA-3' and 5'-TGATTCATCGTGGCACAAAT-3' 57°C annealing temperature, 0:30 elongation time.

Tg(-6.7FRhcrtR:gal4VP16) labels distributed cells in rhomomeres 2-7 of the hindbrain, including neurons in the tangential [S11] and medial vestibular nuclei, and other octavolateral nuclei. There are distributed cells in the spinal cord including the commissural primary ascending (CoPA) neurons. Dispersed cells are visible in the anterior and posterior lateral line, statoacoustic and trigeminal ganglia. In the hypothalamus, the line labels a cluster of cells that

do not overlap with oxytocin, hypocretin or QRFP positive cells. Sparse labeling is detected in the habenula and midbrain tegmentum. Skin and notochord cells are also labeled. See Movie S1.

Tg(14xUAS-E1b:hChR2(H134R)-EYFP): hChR2(H134R)-EYFP [S12] was subcloned downstream of 14 copies of a UAS element and an E1b minimal promoter in a vector containing an SV40 polyA sequence and Tol2 recognition arms [S9]. This vector was co-injected with *tol2 transposase* mRNA into TLAB embryos at the single cell stage. Potential founders were screened by crossing to *Tg(isl1:Gal4-VP16,14xUAS:Kaede)* [S13] and monitoring tail movements in response to blue light from an arc lamp on a stereomicroscope (Leica MZ16) at 30 hours post-fertilization.

Tg(UAS:GCaMP5) was generated by LR recombination of a 14xUAS fragment upstream of *GCaMP5G* and between Tol2 recognition arms, using custom Gateway-compatible entry and destination vectors (Life Technologies). 30 ng/uL of this vector was injected with Tol2 RNA into WIK embryos at the one-cell stage. Potential founders were screened by crossing to *Tg(-6.7FRhcrtR:gal4VP16)*.

The following transgenic lines were used: *Tg(UAS-E1b:Kaede)* [S10], *Tg(UAS:GCaMP-HS)* [S14], and *Et(fos:Gal4-VP16)s1181t* [S15].

Monitoring neural activity by calcium imaging

Calcium imaging was performed with a custom two-photon microscope equipped with a 0.95 NA 20X (Olympus) controlled by custom software written in C# (Microsoft). Z drift was actively compensated by comparing each scanned image to an anatomical reference stack collected immediately prior to imaging. Each newly scanned image was cross correlated in three dimensions with the reference stack using Intel Performance Primitives (IPP) and C#. The lateral search size was ±10 μm and the axial search size was ±5 μm (11 image slices of the reference stack). The depth of the best z slice was low pass filtered and kept within 1 μm of the original focal plane by adjusting the objective height in 1 μm increments. Images were acquired at either 4 or 8 frames a second.

For imaging, 5-6 days post-fertilization (dpf) larvae were paralyzed by soaking in a ~50 μL droplet of 125 mM alpha-bungarotoxin (VWR, 89138-082) for 2 minutes. Fish were then rinsed in E3 and embedded in 2% low-melting point agarose (AquaPor LM, EC-204, National Diagnostics) in E3 for imaging. Neurons were labeled with the genetically-encoded calcium

indicators GCaMP-HS (*Tg(UAS:GCaMP-HS*)) for experiments described in Figures 1 and S1 and with GCaMP5 (*Tg(UAS:GCaMP5*)) for experiments in Figure S4.

Three different types of stimuli were used. Water puffs were delivered through a pipette (either a custom pulled glass pipette of ~0.3 mm inner diameter (IB120F-4, World Precision Instrument) or a blunt tip needle 25G 1½" (Jorgensen Laboratories) delivered ~0.5 mm away from the otic vesicle or the middle of the tail, where a small area was freed of agarose. The strength of the pulse varied from 10 to 40 PSI, with 5-15 ms duration, and was adjusted to obtain a high probability of reliable response without damaging the tissue. Tap stimuli were delivered to the dish holding the larva via a push type solenoid (28-I-12D, Allied Electronics) working with a spring system. The tap produced both a sound and a vibration of the water surrounding the fish. Fish whose probability of response was low or sharply decreased as the experiment progressed were excluded from the analysis (~15%).

Analysis of calcium signals was done in MATLAB (Mathworks, Natick MA). Individual images were first registered in x-y with reference to the first image of an experiment. Regions of interest (ROIs) corresponding to individual neurons or the axon cap were manually drawn. Calcium imaging data is reported as $\Delta f/f$ = (fluorescence over a selected ROI - baseline fluorescence of ROI) / (baseline fluorescence - background fluorescence). Trials for which an ROI showed activity above baseline after the stimulus were scored automatically by the analysis code as response trials and then manually verified.

For experiments combining calcium imaging in the M-cell with laser ablations of spiral fiber neurons, larvae were sequentially stimulated with taps of weak and strong intensity. The difference in magnitude with respect to sound and vibration was not precisely measured. Results were similar with taps of weak and strong intensity. To match the behavior experiments, only results with strong taps are shown. Larvae were paralyzed with alpha-bungarotoxin (Figure S4 A-D). To ensure that the toxin did not influence our experimental outcomes, non-paralyzed fish were also tested (Figure S4 E). No differences in calcium dynamics were observed, and the outcome of the ablations was similar. Post imaging was done starting 10-20 minutes after ablations. Pilot experiments indicated that there was no difference in our results if this interval was prolonged.

High-speed behavioral analysis

A custom-built high-speed video tracking apparatus and custom software written in C# was used to monitor and quantify escape responses to tap stimuli. It consisted of a camera (Pike F-032, Allied Vision Technologies) and variable lens (1:3.9 75 mm, 25.5 mm, Tamron) run at 1000 frames/second by binning pixels, resulting in 104 x 56 images. Larval zebrafish tails were illuminated with IR light. In a manner similar to the calcium imaging experiments, the software sent voltage pulses to a solenoid fixed to the dish holder on which the larva was placed. Different voltages were used to produce taps of three different intensities: small, medium, and strong, which were empirically determined. Because different voltages gave rise to varying stimulus timing, actual tap timing was monitored using a small piezo element (Sparkfun Electronics SEN-10293) mounted close to the solenoid. As recorded by the piezo element, vibration of the dish lasted on the order of 100 ms. A stimulus interval of 20 seconds was used, with which no habituation was observed. Due to the non-directional nature of the stimulus, escapes occurred in either direction. The software tracked tail position online using five equidistant points positioned on the tail. Analysis of tail segment angles was done offline with custom-written scripts in MATLAB. Tail angles reported correspond to the angle of the last tail segment with respect to the vertical. Response latency was defined as the interval between the tap and the first frame at which a tail movement was detected. Tail traces were smoothed using a Butterworth filter (4th order, cutoff = 0.15 Hz). Scripts automatically detected responses and classified them as escapes or non-escapes and detected escape latency. All classifications were then manually verified. Escapes were defined as responses beginning with a turn exceeding 60 degrees in amplitude in the first 25 ms after the stimulus.

To test behavior, 5-7 dpf fish were embedded in 2% low-melting point agarose on a 35 mm diameter petri dish lid, and a scalpel was used to free the tail. A glass cover slip (Gold Seal cover glass, 48x60 mm No.1) was secured with high vacuum grease (Dow Corning) on top of the dish to make a tight water seal and prevent shadows caused by water vibrations. Larvae were allowed to acclimate for at least 30 minutes and then tested individually in the behavioral apparatus for 20 minutes in the dark. Fish were stimulated with the three alternating tap intensities. The outcome of ablations was similar across tap intensities. Only the strongest tap stimulus is shown in Figures 2 and 3 because it elicited the greatest number of escapes. Individual fish whose initial probability of fast escapes averaged over all tap intensities was below 50% were deemed unhealthy and discarded from the analysis (~10% of fish).

Homozygous *mariner* mutants [S16] deficient in hair cell mechanotransduction [S17] were screened based on their lack of a swim bladder, their lying on their side, and their circling movements in response to touch at 4 dpf. Neomycin (neomycin sulfate, Invitrogen 21810-031) treatment was used to kill lateral line neuromasts [S18]. A 50 mM stock solution in E3 was stored at 4°C and diluted 1:100 to use at a final concentration of 500 μM. Larvae were allowed to swim in this solution for 20 minutes and then washed 3 times in E3. Behavioral tests were done no later than 2 hours after treatment to avoid regeneration of neuromasts. Loss of neuromasts was verified on non-tested fish by staining with 2.6 mM DASPEI (2-(4-(dimethylamino)styryl)-N-Ethylpyridinium Iodide, Invitrogen D-426) for 20 minutes [S18].

Experiments involving neuron ablations were done in one day. Baseline responses were recorded in the morning. Larvae were subsequently anesthetized (0.016% w/v tricaine methane sulfonate, Sigma A5040) and placed under a two-photon microscope for neuronal ablations. After the ablation procedure lasting 5-20 minutes, the anesthetic solution was replaced with E3 and larvae were allowed to recover for at least 4 hours and no more than 10 hours before testing their behavior post-ablation.

Laser ablation of neurons

A pulsed two-photon laser was used to ablate specific cells in the M-cell circuit. Laser pulses were focused with a 0.95 NA 20X objective (Olympus) and generated from a Ti:Sapphire system (Spectra Physics MaiTai HP) operating at a 80 MHz repetition-rate with a <100 fs pulse duration. Two methods were used alternatively to achieve neuronal ablation. In one method, the laser was scanned in a spiral pattern over a small area of a selected cell with increasing power [S19]. When brief flashes of high intensity were detected by the software, scanning was automatically stopped. These flashes are thought to arise from absorption of multi-photon energy by water molecules, creating plasma and killing the cell [S20]. An alternative method consisted in sending a single high-power and brief (20-100 ms) pulse. We used a maximum power at sample of 200 mW (820 nm) measured with a power meter (Thorlabs S130C). In most cases, brief flashes of high intensity were observed at the PMT, suggesting plasma formation.

We used different indicators in neurons for ablations: UAS driving ChR2, GCaMP-HS, GCaMP5 or Kaede. Neurons were targeted based on anatomy and were ablated starting with the ventral-most neurons. For M-cell ablations, two locations on the soma were targeted to prevent the cell from recovering. The number of labeled spiral fiber neurons varied by fish between 6-10 cells on

each side. All labeled neurons were targeted, however, it is possible that some ablations were unsuccessful, given the tight packing of cells. Deeper spiral fiber neurons were more challenging to ablate, and sometimes required several attempts with increasing laser pulse lengths. For control ablations, we ablated neurons labeled in *Tg(-6.7FRhcrtR:gal4VP16)* with no apparent connections to the escape circuit and located 20-40 μm rostral and no more than 10 μm away dorsally or ventrally from spiral fiber neuron somata, consisting of 2-6 neurons on each side. Brains were imaged immediately and usually 24 hours after ablation to evaluate the specificity and extent of lesions.

ChR2 stimulation

A 473 nm diode pumped solid state blue laser (DPSSL-473-10, Roithner LaserTechnik) was used to excite ChR2 in heterozygote *Tg(-6.7FRhcrtR:gal4VP16); Tg(UAS:ChR2(H134R)-EYFP)* larvae. The laser beam was focused with a lens on the larva's head to a spot size of approximately 250 μm in diameter (see Figure 4A) with 13 mW power over the sample. 5-7 dpf larvae were embedded in agarose and their tail freed. Escape behavior was then tested in the behavioral apparatus described above, and the tap intensity was optimized for each fish in order to obtain a 5-50% probability of short-latency escapes. Approximately 30 trials were used for each of the following three conditions: 1) low-intensity taps delivered on their own, 2) the same taps paired with a 100 ms blue light pulse delivered 20-60 ms before the taps, and 3) 100 ms light pulses delivered alone. Latency was computed as the time between the onset of the tap and the first movement of the tail, or in the case of the blue light only, from the onset of the light pulse. The delay used between the light and tap in condition 2) was increased if a 20 ms delay did not result in an enhancement of short-latency escapes. For 10/22 ChR2+ larvae, the delay was 20 ms. The mean latency of escapes to blue light only across these fish was 63 ms (± 25 ms standard deviation). For 11/22 fish, the delay was 60 ms and the mean latency of escapes to blue light only across the 7 fish that responded was 92 ms ± 35 ms. One fish was tested with a 40 ms delay and produced escapes with an average latency of 72 ms. Since short-latency escapes occur within 12 ms of the tap, this implies that the escapes assigned as short-latency in condition 2) were generally not caused by the blue alone but by the combination of light and tap (see Figures 4B and S3 E, F and G). It is possible that a subset of long-latency escapes, however, are an effect of the light only stimulus, which could account for the higher probability of long-latency escapes in condition 2) (see Figure S3 A). The delays used for condition 2) in control ChR2- siblings matched in number those used for ChR2+ larvae.

Ablations of spiral fiber neurons were carried out as described above. Larvae were allowed 4-6 hours to recover from the anesthetic before testing post ablation behavior.

Sparse neuron labeling

To label a small number of spiral fiber neurons (Figure 1A), 0.5 nL of 30 ng/μL of plasmid encoding GFP with an N-terminal GAP43 membrane localization sequence [S11] dissolved in water was injected at the one-cell stage into *Tg(-6.7FRhcrtR:gal4VP16)* fish. Embryos were screened under a fluorescent stereoscope (Leica MZ16) with a GFP emission filter. ~10% of embryos had sparse labeling of neurons in the nervous system. The other ~90% either showed no expression or broad expression. Individual spiral fiber neurons were identified by fluorescence at 72 hours post fertilization.

Retrograde labeling of reticulospinal neurons

To label the reticulospinal system including the M-cells, we backfilled neurons from the spinal cord. 5 dpf larvae were anesthetized and placed on a dish filled with solidified 5% agarose. Excess water surrounding the fish was removed with a paper wipe in order to stabilize it. A scalpel was used to sever the spinal cord just caudal of the swim bladder. A sharpened tungsten needle was dipped in a drop of ~40 mM tetramethylrhodamine dextran (Life Technologies, D-3308) whose consistency was adjusted with water to make a gel-like substance. The needle was then placed onto the cut in the spinal cord. Larvae were immediately transferred to E3 and allowed to recover for two hours, while the die filled the reticulospinal system. Their brains were then imaged with a Zeiss LSM 780 NLO microscope used as a confocal.

Immunohistochemistry

For Movie S1, 6 dpf *Tg(-6.7FRhcrtR:gal4VP16); Tg(UAS-E1b:Kaede)* larvae were fixed in 4% PFA in PBT (PBS + 0.25% TritonX), and stained with rabbit anti-Kaede (1:500, PM012, MBL) and mouse anti-ERK1/2 (1:500, #4696, Cell Signaling), and alexa-congugated secondary antibodies (1:500, goat anti-mouse IgG Alexa Fluor® 647, A-21235 and goat anti-rabbit IgG Alexa Fluor® 546, A-11035, Life Technologies). Fish were imaged by confocal microscopy using a 20x 1.0 NA objective.

Statistics

Significance was determined using the Wilcoxon signed rank test for paired data and the Wilcoxon rank sum test for independent samples. All data are reported as mean ± standard error of the mean.

SUPPLEMENTAL REFERENCES

S1. Kimmel, C. B., Powell, S. L., and Metcalfe, W. K. (1982). Brain neurons which project to the spinal cord in young larvae of the zebrafish. J Comp Neurol *205*, 112–127.

S2. Koyama, M., Kinkhabwala, A., Satou, C., Higashijima, S.-I., and Fetcho, J. (2011). Mapping a sensory-motor network onto a structural and functional ground plan in the hindbrain. Proc Natl Acad Sci USA *108*, 1170–1175.

S3. Scott, J. W., Zottoli, S. J., Beatty, N. P., and Korn, H. (1994). Origin and function of spiral fibers projecting to the goldfish Mauthner cell. J Comp Neurol *339*, 76–90.

S4. Kohashi, T., and Oda, Y. (2008). Initiation of Mauthner- or non-Mauthner-mediated fast escape evoked by different modes of sensory input. J Neurosci *28*, 10641–10653.

S5. O'Malley, D. M., Kao, Y.-H., and Fetcho, J. R. (1996). Imaging the functional organization of zebrafish hindbrain segments during escape behaviors. Neuron *17*, 1145–1155.

S6. Satou, C., Kimura, Y., Kohashi, T., Horikawa, K., Takeda, H., Oda, Y., and Higashijima, S.-I. (2009). Functional role of a specialized class of spinal commissural inhibitory neurons during fast escapes in zebrafish. J Neurosci *29*, 6780–6793.

S7. Kohashi, T., Nakata, N., and Oda, Y. (2012). Effective Sensory Modality Activating an Escape Triggering Neuron Switches during Early Development in Zebrafish. J Neurosci *32*, 5810–5820.

S8. Furshpan, E. J., and Furukawa, T. (1962). Intracellular and extracellular responses of the several regions of the Mauthner cell of the goldfish. J Neurophysiol *25*, 732–771.

S9. Urasaki, A., Morvan, G., and Kawakami, K. (2006). Functional dissection of the Tol2 transposable element identified the minimal cis-sequence and a highly repetitive sequence in the subterminal region essential for transposition. Genetics *174*, 639–649.

S10. Scott, E. K., Mason, L., Arrenberg, A. B., Ziv, L., Gosse, N. J., Xiao, T., Chi, N. C., Asakawa, K., Kawakami, K., and Baier, H. (2007). Targeting neural circuitry in zebrafish using GAL4 enhancer trapping. Nat Methods *4*, 323–326.

S11. Bianco, I. H., Ma, L.-H., Schoppik, D., Robson, D. N., Orger, M. B., Beck, J. C., Li, J. M.,

Schier, A. F., Engert, F., and Baker, R. (2012). The tangential nucleus controls a gravito-inertial vestibulo-ocular reflex. Curr Biol *22*, 1285–1295.

S12. Zhang, F., Wang, L.-P., Brauner, M., Liewald, J. F., Kay, K., Watzke, N., Wood, P. G., Bamberg, E., Nagel, G., Gottschalk, A., et al. (2007). Multimodal fast optical interrogation of neural circuitry. Nature *446*, 633–639.

S13. Pan, Y. A., Choy, M., Prober, D. A., and Schier, A. F. (2012). Robo2 determines subtype-specific axonal projections of trigeminal sensory neurons. Development *139*, 591–600.

S14. Muto, A., Ohkura, M., Kotani, T., Higashijima, S.-I., Nakai, J., and Kawakami, K. (2011). Genetic visualization with an improved GCaMP calcium indicator reveals spatiotemporal activation of the spinal motor neurons in zebrafish. Proc Natl Acad Sci USA *108*, 5425–5430.

S15. Scott, E. K., and Baier, H. (2009). The cellular architecture of the larval zebrafish tectum, as revealed by gal4 enhancer trap lines. Front. Neural Circuits *3*, 13.

S16. Nicolson, T., Rüsch, A., Friedrich, R. W., Granato, M., Ruppersberg, J. P., and Nüsslein-Volhard, C. (1998). Genetic analysis of vertebrate sensory hair cell mechanosensation: the zebrafish circler mutants. Neuron *20*, 271–283.

S17. Ernest, S., Rauch, G. J., Haffter, P., Geisler, R., Petit, C., and Nicolson, T. (2000). Mariner is defective in myosin VIIA: a zebrafish model for human hereditary deafness. Hum. Mol. Genet. *9*, 2189–2196.

S18. Harris, J. A., Cheng, A. G., Cunningham, L. L., MacDonald, G., Raible, D. W., and Rubel, E. W. (2003). Neomycin-Induced Hair Cell Death and Rapid Regeneration in the Lateral Line of Zebrafish (Danio rerio). JARO - Journal of the Association for Research in Otolaryngology *4*, 219–234.

S19. Orger, M. B., Kampff, A. R., Severi, K. E., Bollmann, J. H., and Engert, F. (2008). Control of visually guided behavior by distinct populations of spinal projection neurons. Nat Neurosci *11*, 327–333.

S20. Vogel, A., and Venugopalan, V. (2003). Mechanisms of pulsed laser ablation of biological tissues. Chem. Rev. *103*, 577–644.